"BABEȘ-BOLYAI" UNIVERSITY CLUJ-NAPOCA
FACULTY OF ENVIRONMENTAL SCIENCE AND ENGINEERING
DOCTORAL SCHOOL OF ENVIRONMENTAL SCIENCE

PhD THESIS SUMMARY

The Hybrid Solution: Efficient Wastewater Remediation With Innovative Sustainable Adsorbents

PhD Student:
Iolanda-Veronica GANEA

PhD Coordinator:
Prof. Univ. Dr. Laurențiu-Călin BACIU

Cluj-Napoca,
2025

THESIS TABLE OF CONTENTS

LIST OF ABBREVIATIONS AND ACRONYMS

AAS – Atomic Absorption Spesctroscopy

BET – Brunauer-Emmett-Teller Analysis

BP – Banana peel

BPSD – Composite based on banana peel and stone dust

CG – Coffee grounds

CHIT - Chitosan

CHIT-PAAA - chitosan modified with poly(benzofurane-*co*-arylacetic acid)

DA – Dopamine

DLS – Dynamic Light Scattering

EC – Electrical Conductivity

FA – Folic acid

FTIR - Fourier-Transform Infrared Spectroscopy

MMT - Montmorillonite

MMT-PBAAA - Montmorillonite modified with poly(benzofurane-*co*-arylacetic acid)

MMT-PBAAA-DA - Montmorillonite modified with poly(benzofurane-*co*-arylacetic acid) functionalized with dopamine

MNPs - Magnetic nanoparticles

MNP@PAAA-DA - Magnetic nanostructures based on poly(benzofurane-*co*-arylacetic acid) functionalized with dopamine

MNP@PAAA-FA – Magnetic nanostructures based on poly(benzofurane-*co*-arylacetic acid) functionalized with folic acid

MNP@PAAA-NTA - Magnetic nanostructures based on poly(benzofurane-*co*-arylacetic acid) functionalized with Nα, Nα'–bis(carboxymethyl)-L-lysine

MNS – Magnetic nanostructures

NTA - Nα, Nα'–bis(carboxymethyl)-L-lysine

ORP – Oxidation – Reduction Potential

PAAA-CL-XLD - Poly(benzofurane-co-arylacetic acid) crosslinked with *p*-xylenediamine

PAAA-DA - Poly(benzofurane-*co*-arylacetic acid) functionalized with dopamine

PAAA-NTA - Poly(benzofurane-*co*-arylacetic acid) functionalized with Nα, Nα'–bis(carboxymethyl)-L-lysine

PBAAA – Poly(benzofurane-*co*-arylacetic acid)

pH - Logarithmic scale used to specify the acidity or alkalinity of an aqueous solution

S – Salinity

SD – Stone dust

ss-NMR – Solid-State Nuclear Magnetic Resonance Spectroscopy

SEM – Scanning Electron Microscopy

TDS – Total Dissolved Solids

TEM – Transmission Electron Microscopy

TGA – Thermogravimetric Analysis

UV-VIS – Ultraviolet-Visible Spectroscopy

VSM - Vibrating-Sample Magnetometry

XRPD – X-Ray Powder Diffraction Analysis

XPS – X-Ray Photon Electron Spectroscopy

ZD – Zein-DMAB nanoparticles

ZT – Zein-Tween80 nanoparticles

WR – Watermelon rind

WRCG – Composite based on watermelon rind and coffee grounds

WRSD – Composite based on watermelon rind and stone dust

Keywords: *water pollution, metal contamination, dyes pollution, hybrid materials, wastewater remediation, innovative green adsorbents, eco-innovative nanostructures, sustainable biopolymers, environmentally-friendly mineral composites, circular waste-based composites*

INTRODUCTION

British astronomer Royal Professor Sir Martin Rees highlighted in his 2010 BBC Reith Lectures "Scientific Horizons" the extraordinary impact that mankind has now on the future of our planet: "*This is a crucial century. The Earth has existed for 45 million centuries. But this is the first when one species, ours, can determine – for good or ill – the future of the entire biosphere*" (Rees, 2010). This quote suggests that humanity has reached a pivotal moment in history, when our actions have the potential to either protect or permanently damage the environment and, therefore, all living forms reliant on it. Considering the growing environmental challenges, it is our responsibility to start focusing more on finding new ways to protect "our home".

In particular, water resources, which are one of the essential elements for sustaining life, are under increased threat. Global population increase and agricultural and industrial activities have made a substantial contribution to water contamination. According to (Esrey et al., 1991) and (WaterAid & Tearfund, 2001) insufficient sanitation, lack of access to water supplies and contaminated water cause 80% of all diseases in developing countries. The American President Lyndon B. Johnson warned about the dangers of neglecting the proper management of water resources in a letter to the President of the Senate and Speaker of the House from 1968, stating: "*A nation that fails to plan intelligently for the development and protection of its precious waters will be condemned to wither because of its shortsightedness. The hard lessons of history are clear, written on the deserted sands and ruins of once proud civilizations*" (Johnson, 1968). The use of the terms "*deserted sands and ruins*" highlights the fact that the failure to manage water wisely could lead even to the collapse of civilizations similar to other past events in humanity's history. In the last century, this environmental factor has become a vulnerable resource, therefore, its

management and protection have become top priorities worldwide. Despite all progresses made in the development of new materials for wastewater treatment, existing adsorbents often have limitations related to their efficiency, costs or toxicity concerns. In this context, there is an urge to support the eco-initiatives that promote a clean environment, and the wastewater decontamination challenges using "*green solutions*".

Based on this premise, the **theme of the current thesis** entitled "*The Hybrid Solution: Efficient Wastewater Remediation With Innovative Sustainable Adsorbents*" centres on the development of innovative materials and the assessment of their potential for usage in wastewater treatment, merging the fields of environmental protection, materials science, and public health. **The thesis aims** to address the above-mentioned challenges by conducting an integrated study on four categories of novel materials with applications in environmental protection, combining their synthesis, characterization and applications in decontamination.

The general objective of this thesis consisted in the development of a complete cycle, starting from the preparation and characterization of the new materials to their application in the adsorption of several types of pollutants from contaminated waters in order to reduce exposure and associated risks to human health.

The specific objectives established in the present research have been achieved and involved: (i) synthesizing the four categories of materials via "*green chemical methods*", (ii) characterizing them through various structural and morphological techniques, (iii) evaluating their adsorption performance on inorganic (heavy metals) and organic pollutants (synthetic dyes) and (iv) investigating and modelling the adsorption mechanisms.

This thesis is **structured in four chapters**, as follows: **Chapter 1** includes the theoretical context highlighting the growing problem of water pollution and the need for innovation in the field of wastewater treatment, as well as the scientific literature review regarding materials used for wastewater decontamination. **Chapter 2** details the materials and experimental design used in this research, including the materials' synthesis and characterization methods, the protocols to assess their adsorption performance after their application. **Chapter 3** presents the experimental results obtained after conducting the steps previously mentioned and includes descriptions of each material and the characterization of their structural and morphological properties, the outputs of the adsorption performance tests, as well as comparative discussions between the results of the current research and other materials reported in the scientific literature. **Chapter 4** summarizes the

key findings, outlining their contributions to the field, and providing recommendations for future research.

The importance of conducting this type of studies is essential, considering the serious threat that water contaminants present to both ecosystems and human health. The current research **significantly contributes to the field of wastewater treatment and environmental protection** by exploring the potential of sustainable innovative materials to enhance water quality while prioritizing human health safety. The findings can have broad applications in environmental remediation, providing safer alternatives to existing wastewater treatment methods. This research **supports the current national and international efforts to guarantee clean and safe water**, in line with the sustainability and circular economy principles, as well as with the United Nations Sustainable Development Goals (SDGs), namely SDG 6 (Clean Water and Sanitation) and SDG 4 (Good Health and Well-Being).

1. THEORETICAL CONTEXT AND LITERATURE REVIEW

1.1. Water Resources: Availability, Distribution and Importance

Water is among the most abundant molecules on Earth and is comprised of one atom of oxygen and two atoms of hydrogen covalently bonded (Lerner & Wilmoth Lerner, 2005). It is an essential resource for all forms of life and for many economic sectors such as agriculture, energy production, industrial operations and recreational activities (Booth & Charlesworth, 2014). The planet's surface is covered by water to an extent of 71%, with 97.5% of it representing sea water (Ahuja, 2021). Freshwater accounts for less than 3% of the total water resources available worldwide and is distributed unequally, America and Asia benefiting from the largest shares (45% and 28%, respectively) among all continents (Musie & Gonfa, 2023). Only 0.3% of the total freshwater available is easily accessible in the form of reservoirs, the remaining being stored as groundwaters, soil moisture and swamps (30.8%) or glaciers (68.9%) (Rijsberman, 2006).

Global water supplies are nowadays under considerable pressure due to population growth, intensive agricultural practices and industrialization. Experts often mention that we are approaching the "peak water", concept referring to the threshold of safe water withdrawal needed to ensure sufficient water supplies remain to sustain the aquatic ecosystems and biodiversity (Norton et al., 2018). Water scarcity appears when the amount of water consumed is insufficient to meet the society's demands (Lehr et al., 2005). The International Water Management Institute reported that 2.7 billion people face water shortage in 2025 and 3.2 billion are estimated to live under severe water scarcity conditions by 2050 (Molden, 2007). In addition to the water scarcity problem, there is also another significant challenge that poses a threat to global resources, namely the degradation of its quality via pollution (Du Plessis, 2023). Currently, there are more than 2.2 billion people (mostly in developing countries) accounting for 27% of world's population that do not have yet access to clean water, resulting in numerous cases of individuals suffering from diseases associated with waterborne pathogens (United Nations, 2015; United Nations Water, 2021). Therefore, it is essential to address these issues and guarantee the basic right for safe water to all humans, as highlighted by The United Nations General Assembly in 2010 and stipulated in SDG 6 Clean Water and Sanitation (United Nations' General Assembly, 2010; Hall et al., 2014).

1.2. Water Quality

General Parameters

The term "water quality" indicates the optimum condition of the key water parameters that determines its suitability for a specific application (Hutzinger et al., 2009). The main water quality indices widely monitored are: pH, dissolved oxygen, total dissolved solids, biochemical oxygen demand, chemical oxygen demand, turbidity, salinity, conductivity nutrients, heavy metals, pesticides, microorganisms.

Water Quality Legislation

Different legislative frameworks are implemented on national and international levels for the protection of water quality, establishing guide levels, maximum admissible concentrations and minim required concentrations (Geerten, 1998). The Clean Water Act (United States Environmental Protection Agency (US EPA), 1972) and The Safe Drinking Water Act (United States Environmental Protection Agency (US EPA), 1974) are the main regulatory water policies in USA. In EU, more than 25 directives and decisions on fresh and sea water pollution have already been adopted, however, The Water Framework Directive (2000/60/EC) (European Commission, 2000) represents the fundamental and most integrative water policy formulation. Romania aligned with the European legislation for the management of water quality as well by implementing the EU's water directives through various national frameworks, like: Waters Law No. 107 from 25/09/1996 (Parliament of Romania, 1996), Law No. 458 from 08/07/2002 , Law No. 311 from 28/06/2004 and Ordinance No. 7 from 18/01/2023 on the quality of water intended for human consumption (Government of Romania, 2023; Parliament of Romania, 2002; Parliament of Romania, 2004), etc.

1.3. Water Pollution

Overview

Water pollution represents the deterioration of the physical, chemical or biological properties of water, that triggers the degradation of its quality and the negative impact on living organisms. According to the 20th Edition of The Global Risks Report from (The World Economic Forum, 2025), environmental risks present the highest degradation, being expected to worsen in

severity over the next two/ten years with an alarming rate. Pollution ranks on the 5th position among the top 33 risks worldwide perceived by society to have a dangerous short-term impact (The World Economic Forum, 2025).

Types of Pollutants in Water

Water pollutants refer to any substances or materials that alter its quality and applications by exceeding the maximum permissible thresholds recommended (Negulescu et al., 1982). Water can contain a large variety of contaminants grouped into various categories based on their nature: physical/chemical/biological or inorganic/organic/biotic, primary/secondary, natural/anthropogenic, etc. (Török & Dransfield, 2017). The sources of pollution can also be classified according to their origin (natural/anthropogenic), distribution (point/dispersed/transboundary). duration (permanent/ accidental/temporary) (Török & Dransfield, 2017). While certain contaminants are also naturally released into the environment through geological and biological processes, anthropogenic activities tend to have the most significant input to water pollution (Crini et al., 2019).

Heavy Metals

The term "heavy metal" is typically attributed to metals and metalloids with densities exceeding 5 g cm^{-3} (Lichtfouse et al., 2012). About 90 metals are encountered in the environment, however only 53 are considered heavy metals (e.g. Ag, As, Au, Be, Cd, Co, Cr, Cu, Fe, Ga, Ge, Hg, In, Mn, Ni, Pb, Pd, Pt, Sb, Se, Sn, Tl, Zn). Most heavy metals pose a significant risk to public health since they are toxic, persistent and tend to easily accumulate in aquatic organisms and further transfer to humans via food chain (M. Hussain et al., 2025). However, some of them (e.g. Fe, Mn, Cu) are considered "essential elements" being necessary for organisms in low concentrations. Sources of heavy metals in the water include burning fossil fuels, mining and smelting metallic ferrous ores, municipal wastes, fertilizers, pesticides, sewage sludge, etc. (Lichtfouse et al., 2012). The major industrial sectors that contribute to this type of pollution are the steel and textiles manufacturing, electroplating and leather tanning (Hussain et al., 2025). Modern mining generates large amounts of tailings and waste rocks that have the potential to induce significant environmental changes (United Nations Environment Programme, 2019).

1. THEORETICAL CONTEXT AND LITERATURE REVIEW

Dyes

Dyes represent a category of organic xenobiotics that had a massive expansion among textile, leather, plastics, food, pharmaceuticals and paints manufacturing industries in the past few years (Lichtfouse et al., 2012). Each dye selectively absorbs specific wavelengths of light, resulting in its colouration. They include two essential components. chromophores (unsaturated functional groups that confer colour, like –N=N–, –C=C–, –C=N–, and –C=O) and auxochromes (units that enhance the chromophore's coloring effect and increase the molecule's solubility in water, such as –OH, $–NH_2$, –NHR, $–NR_2$, $–NO_2$, –OR, –COOH, –CHO, and $–SO_3$) (Crini & Lichtfouse, 2018). Dyes are classified based on their origin (natural/synthetic), colour, application, charge (anionic/cationic) or chemical structure (ionic/non-ionic). The intensive industrialization triggered a massive development in the synthetic dyes field, more than 10000 colorants and pigments being commercially available nowadays (Bilal et al., 2021). It is estimated that each year over 150000 tonnes of residual dyes involved in manufacturing get released in the environment without any prior treatment (Lichtfouse et al., 2012). This accounts for approximately 1500 million L of dye-contaminated effluents being discharged daily into various environmental systems (Ganea et al., 2021).

Effects Induced by Water Pollution

Water pollution negatively impacts wildlife, marine ecosystems and human health, by generating habitat loss or degradation and proliferation of invasive species and pathogens (Balaram et al., 2023). Pollutants can inhibit the growth or cause the death of aquatic species, leading to the prolonged deterioration of aquatic environments and reduction in the diversity and species abundance (Malmqvist & Rundle, 2002).

Human exposure to heavy metals in waters induces acute and chronic effects, disturbing the normal functioning of nervous, respiratory, digestive, renal and reproductive systems (El Mahdaoui et al., 2024). Chromium (VI) is a strong oxidising agent and carcinogen, presenting considerable health hazards to people and animals, including cancer, epigastric discomfort, nausea, severe diarrhoea, vomiting, and haemorrhage (Barnhart, 1997). Cadmium, recognised as a human carcinogen, is associated with renal impairment, bone demineralisation, and several health complications (Godt et al., 2006). Copper in, excess can lead to toxicity and carcinogenic effects, resulting in liver and kidney failure, headaches, and vomiting (Georgopoulos et al., 2001). Nickel,

another carcinogenic substance, may result in renal and pulmonary issues, gastrointestinal disturbances, and dermatological diseases (Bennett, 1982).

Water that contains dyes, even in low concentrations (1.0 mg L^{-1}) is considered unsuitable for human consumption (Velusamy et al., 2021). In general, these pollutants are non-degradable, toxic and carcinogenic, causing acute and chronic effects like allergies, cardiovascular diseases, mutations, tumors, etc. (Xu et al., 2010). Azo dyes are reduced to aromatic amines (aryl amines) by azo reductases in liver and kidneys cells, skin and intestinal bacteria (Dutta et al., 2024). Epidemiological studies have demonstrated that prolonged occupational exposure to aromatic amines like benzidine, 4-aminobiphenyl, and 2-naphthylamine, utilized in dye industries, increases the chance to develop cancer.

1.4. Wastewater Treatment Processes

Generalities

The continuous use of vast categories of chemical compounds had shifted mankind from the Industrial Revolution Era to the "*Pollutant Removal Age*", characterized by significant efforts towards creating new materials and technologies to reduce emissions. Wastewater treatment processes can be classified into physical, chemical and biological or primary, secondary or tertiary. Physical treatment refers to sedimentation, flotation, and filtration, chemical treatment implies coagulation, flocculation and advanced oxidation processes, whereas biological treatment uses microorganisms to convert dissolved organic matter into biomass via activated sludge, trickling filters, and bioreactors (Wrobel & Brebbia, 1991). Advanced treatment methods include more complex processes such as reverse osmosis and electrodialysis (Hussain et al., 2025). Despite all the progress made in this field, the conventional treatment methods tend to either have high costs of treatment, use large amounts of chemicals, generate toxic secondary products, be less accessible, etc. (Lichtfouse et al., 2012).

Adsorption Process

In this context, adsorption arised as a promising option, providing a strong balance between the environmental and economic aspects (Hussain et al., 2025). Adsorption is the process by which substances (adsorbates) bind to a solid material forming a thin layer (substrate) (Crini et al., 2019). Physical adsorption implies the presence of hydrogen bonding, weak van der Waals forces, and

electrostatic attractions, whereas chemical adsorption involves the formation of new chemical bonds between adsorbents and adsorbates (Saleh, 2024). Recently, researchers increased focused towards "green adsorption" processes denoting the use of adsorbents synthesized through "*green chemical methods*" and biosorption which refers to the removal of substances from solution by adsorption onto biologically derived materials, such as biomass, fibers, peat, chitosan, algae, plant or animal waste (Vijayaraghavan & Balasubramanian, 2015).

Regarding the adsorption parameters, it is well-known that pH can affect the activity of the functional groups present in the adsorbent (the surface charge) and the solution's chemistry (influencing metals speciation, electrostatic interactions) (El Mahdaoui et al., 2024). Positively surface charges under acidic conditions lead to the protonation of functional groups, promoting anion attraction, whereas negatively charged surfaces attract cations. Materials with low surface charges have better absorbance performances for anions at lower pH and for cations at higher pH. The initial concentration of contaminant also impacts the adsorption mechanism, larger amounts triggering higher sorption capacities due to more molecules coming into contact with the materials surface (Hussain et al., 2024). Temperatures between 20–35 °C have a minor influence on adsorption, however higher values often tend to increase surface activity and kinetic energy. On the other hand, an increase in ionic strength usually enhances the adsorption's efficiency. Adsorbent dosage can also impact the sorption capacity due to the increased or diminished availability of binding sites in the materials (El Mahdaoui et al., 2024). The effect of contact time is proportional with the sorption capacity since more interactions occur between the contaminants in the solution and the free active sites in the materials. The stirring speed plays an important role on adsorption efficiency as well, elevated values enhancing the performance due to the higher collision frequency between the molecules of contaminant and the active sites of the materials. Competing ions in the matrix reduce the sorption capacity, affecting the selectivity of the adsorbent.

Heavy Metals Adsorption

Researchers have been developing different biosorbents for heavy metals in the past few decades from bacteria (Pham et al., 2022), fungi (Kumar et al., 2019) magnetic biomaterials (Nejadshafiee & Islami, 2019), nanocellulose (Jiang et al., 2023), lignin (Zhang et al., 2023), plant or animal waste (Bilal et al., 2021), etc. The last category of adsorbent materials promotes circular economy by transforming waste into a valuable resource that supports environmental cleaning (Guechi & Hamdaoui, 2016).

1. THEORETICAL CONTEXT AND LITERATURE REVIEW

Dyes Adsorption

Various adsorbents have been reported in the scientific literature for the removal of dyes, such as: commercial activated carbon (Malik, 2004), waste-based activated carbon (Ding et al., 2014), agricultural wastes (coffee ground powder, sawdust, leaves, etc.) (Crini, 2006), industrial wastes (fly ash, slurry, ceramic waste, etc.) (Jain et al., 2003), clays and zeolites (kaolinite, montmorillonite, palygorskite, Saklikent mud) (Santos & Boaventura, 2008), cellulose (Liu et al., 2015), biomass (Dotto et al., 2012), hybrid nanomaterials (carbon-based hybrid nanocomposites, carbon nanotubes, graphene and reduced graphene oxide nanocomposites, etc.) (Yang et al., 2011), metal oxide-based hybrid materials (magnetic and non-magnetic) (Liu et al., 2014), metal-organic frameworks (MOFs) (Haque et al., 2013), or polymers and nanocomposites (polyaniline, polypyrrole, chitosan, etc.) (Janaki et al., 2012).

Importance of Wastewater Decontamination

Wastewater treatment brings significant benefits to many different fields, such environmental protection, public health, economy, etc. This process is essential for maintaining the ecological balance that supports aquatic life (Carpenter et al., 1998), reducing the transmission of waterborne diseases and protecting population health (World Health Organization (WHO), 2017), decreasing pressure and demand on water supplies needed for various activities (irrigation, energy production, industrial processes, daily population consumption) (Mekala et al., 2008).

2. Data Processing and Mapping of Scientific Literature

The current thesis includes also a bibliometric analysis, providing an historical overview on the scientific progress made in the field of materials used for heavy metals and dyes adsorption from wastewater. The bibliometric maps generated focus on the investigation of keywords co-occurrence, co-authorship and citation/co-citation indicating the research trends, the existing collaborative networks between authors/countries and the relationships between the publications cited together.

2.1. Bibliometric Analysis on Materials for Heavy Metals Adsorption

The assessment of the trend in scientific articles on materials applied for heavy metals adsorption published in the past two decades. Thus, it can be noticed that the number of publications in this field grew significantly between 2016-2024 (accounting for 71.7% of the total amount of papers published), as a result of the research funding supplementations and raised awareness of the environmental and health hazards associated with the exposure to heavy metals. The co-occurrence map provides an overview of the most used terms in the titles, abstracts and keywords sections of the research related to materials applied for heavy metals decontamination published between 1st of January 2005 and 31st of December 2024. This map includes four major keywords clusters denoting various themes, such as: adsorbent materials synthesized (red cluster), analytical techniques applied (yellow cluster), heavy metals targeted for adsorption (green cluster) and characteristics of the sorption process (blue cluster). The co-authorship density map provides important information on the main contributors in the field of materials applied for heavy metals adsorption in the last two decades. The node representing Zhang Y. highlights the central part of the map, indicating this author has been involved in numerous collaborations, contributing significantly to the scientific literature on adsorbents for heavy metals removal. The geographic distribution of papers related to adsorbents used for retention of heavy metals in wastewaters, published between 2005-2024, emphasizes that Asia exhibits the largest number of publications on this topic, being followed by Europe and North America. At the opposite end is Africa with the lowest representation and amount of articles published due to the insufficient resources and infrastructure allocated. The citation map of the research environment on adsorbents for heavy metals decontamination shows that papers like (Chandra et al., 2010) and (Zhao et al., 2011) have the largest nodes (with more than 1400 citations), indicating that they built the foundation for future

research. The co-citation map provides a comprehensive view on the relationships between articles, authors and thematic groups in the field of adsorbents for heavy metals retention during the last two decades. Papers like (Langmuir, 1918), (Temkin & Pyzhev, 1940) and (Ho & McKay, 2000) have been highly influential, reflecting studies that have played a fundamental role in the development of the adsorption mechanism theories related to equilibrium and kinetics.

2.2. Bibliometric Analysis on Materials for Dyes Adsorption

The trend analysis on the scientific articles related to materials used for dyes adsorption published between 1st of January 2005 and 31st of December 2024, can be divided into two major periods, as follows: first one with a gradual increase (between 2005-2014, representing 16% of the total amount of papers published) and last one with an exponential growth (between 2015-2024, counting for 84% of the total number of publications). The co-occurrence map that analyzes the frequency of the main terms mentioned together in the title, abstracts and keywords of scientific articles published between 1st of January 2005 and 31st of December 2024 regarding materials used for dyes adsorption can be divided into four major clusters, each representing a distinct topic in the field of materials applied for dyes removal: adsorbent materials and techniques (red cluster), sorption mechanism characteristics (green cluster), adsorption of specific dyes (purple cluster) and synthesis and surface modifications of adsorbent materials (blue cluster). The co-authorship density map which highlights the collaboration patterns over the past twenty years among authors in the field of materials with applications in dyes adsorption from wastewater shows that the main authors with extensive collaboration networks, likely influential in the investigated field, are Liu Y., Dotto G.L., Ghaedi. M., and Jawad A.H. The geographic distribution of the scientific papers related to materials for dyes adsorption in regions such as North America, Europe, and Asia is dispersed, different countries contributing at varying scales based on the local needs, financial resources, and research priorities. The co-citation map highlights the citation patterns of scientific articles related to materials for dyes adsorption in the past two decades. Strong co-citation values (ranging between 2000-5000 citations and 30000-50000 total link strength) were noticed between (Langmuir, 1918), (Ho & McKay, 2000), (Freundlich, 1907), (Lagergren & Sven, 1898) and (Weber & Morris, 1963), suggesting that adsorption isotherms and kinetic models are frequently discussed together with dyes adsorption studies in the scientific literature.

2. MATERIALS AND METHODS

2.1. Data Processing and Mapping of Scientific Literature

This section presents the complete description of the research methodology applied for data processing and mapping of scientific literature. The PRISMA approach (Haddaway et al., 2022) was used in this regard on records reported between 2005-2024 in two databases: Web of Science (WoS) and Scopus. Maps were generated with VOSviewer version 1.6.20 (Centre for Science and Technology Studies Leiden University (CWTS), Leiden, The Netherlands) based on keywords co-occurrences, co-authorship, citation and co-citation networks and were designed to accurately highlight the main themes or trends in the materials science research field and the relationships between scientific publications on this topic and their authors.

2.2. Chemicals and Reagents

The synthesis of **PBAAA** and **MNPs** were performed following previously reported procedures (Nan et al., 2017; Nan et al., 2019). The stock solutions employed in the adsorption experiments were obtained using $CuSO_4$, $ZnSO_4 \times 7H_2O$, $MnSO_4 \times H_2O$, $CdCl_2 \times H_2O$, $PbCl_2$, $Fe_2(SO_4)_3 \times 5H_2O$, $CrCl_3 \times 6H_2O$, anhydrous $NiCl_2$ and ultrapure water (pH 5.5) produced with a Milli-Q equipment (Millipore, Bedford, MA, USA). All reagents used were acquired from Sigma Aldrich (St. Louis, MO, USA) and Alfa Aesar by ThermoFisher Scientific (Kandel, Germany) and did not necessitate additional purification, unless otherwise stated.

2.3. Materials Synthesis Procedures

This stage involved the application of "green" chemical synthesis methods specific to each type of material. The chemical methods used followed the principles of sustainable development and circular economy to ensure cost-effectiveness and reliability. ten materials were synthesized during the PhD research and can be classified in four categories:

A. Eco-Innovative Nanostructures (core-shell magnetic nanostructures based on poly(benzofuran-co-arylacetic acid) functionalized with Nα, Nα'–bis(carboxymethyl)-*L*-lysine (**MNP@PAAA-NTA**); core-shell magnetic nanostructures based on poly(benzofuran-co-arylacetic acid) functionalized with dopamine (**MNP@PAAA-DA**); core-shell magnetic

nanostructures based on poly(benzofuran-co-arylacetic acid) functionalized with folic acid (**MNP@PAAA-FA**); zein-based polymeric nanostructures (**ZD** and **ZT**))

B. Sustainable Biopolymers (chitosan modified with PBAAA (**CHIT-PAAA**) and poly(benzofurane-co-arylacetic acid) crosslinked with p-xylenediamine (**PAAA-*CL*-XLD**))

C. Environmentally-Friendly Mineral Composites (montmorillonite modified with poly(benzofurane-co-arylacetic acid) functionalized with dopamine (**MMT-PBAAA-DA**))

D. Circular Waste-Based Composites (composite based on banana peel and stone dust (**BPSD**); composite based on watermelon rind and coffee grounds (**WRCG**); composite based on watermelon rind and stone dust (**WRSD**))

2.4. Instrumentation

2.4.1. Fourier-Transformed Infrared Absorption Spectroscopy (FTIR)

A JASCO FTIR-6100 spectrophotometer (JASCO Deutschland GmbH, Pfungstadt, Germany) was used to capture infrared absorption spectra in the 400–4000 cm^{-1} spectral range on a pressed pellet made from the powdered samples embedded in KBr. The spectrophotometer is capable of determining the presence of various chemical bonds in the structure of the prepared materials and is equipped with software that releases FTIR spectra and highlights molecular vibrational peaks.

2.4.2. Transmission Electron Microscopy (TEM), Scanning Electron Microscopy (SEM) and Energy-Dispersive X-Ray Spectroscopy

A Hitachi HD-2700 Scanning Transmission Electron Microscope (STEM) and a Hitachi SU8230 High Resolution Scanning Electron Microscope (Hitachi Ltd., Tokyo, Japan) were used to determine the samples' morphology. Hitachi HD-2700 Scanning Transmission Electron Microscope is equipped with a cold field emission gun, working at an acceleration voltage of 200 kV and designed for high-resolution (HRTEM) imaging with a resolution of 0.144 nm. A 10 µl drop of suspension of each sample was deposited and dried on a copper grid coated by a thin carbon film prior to the electron microscopy analysis. Hitachi SU8230 High Resolution Scanning Electron Microscope is equipped with a cold field emission gun. For morphological analysis the samples was deposited on aluminum stubs and coated with a 10 nm gold layer.

2.4.3. Magnetic Measurements (VSM)

Magnetic measurements were conducted at room temperature utilising a Vibrating Sample Magnetometer (Cryogenic Ltd., London, UK).

2.4.4. Thermogravimetric Analysis (TGA)

Thermogravimetric measurements were conducted in air at a heating rate of 10°C min^{-1} between 30 °C and 800 °C using a TA Instruments SDT Q 600 equipment (TA Instruments Inc., New Castle, DE, USA) (Ganea et al., 2021).

2.4.5. X-ray Powder Diffraction Analysis (XRPD)

X-ray powder diffraction (XRPD) measurements were carried out at room temperature using a LynxEye position sensitive detector (Bruker, Karlsruhe, Germany) and a Bruker D8 Advance X-ray diffractometer (Bruker, Billerica, MA, USA) equipped with a Ge (111) monochromator for Cu-Kα1 radiation (λ = 1.5406 Å) with source power of 40 kV and 40 mA. The diffraction pattern was monitored in the 2θ range of 10 to 90 with a scan step of 0.02° and a scan speed of 1° min^{-1} to record the experiments (Ganea et al., 2021).

2.4.6. X-Ray Photon Electron Spectroscopy (XPS)

An XPS spectrometer from SPECS Surface Nano Analysis GmbH (Berlin, Germany), equipped with a dual-anode X-ray source (Al/Mg), a PHOIBOS 150 2D CCD hemispherical energy analyser, and a multi-channeltron detector with a vacuum maintained at 1 x 10^{-9} torr, was utilised to acquire XPS spectra. The analyses were performed with an Al Kα X-ray source (1486.6 eV) operating at a power of 200W. The XPS survey spectra were captured at a pass energy of 30 eV, with a step size of 0.5 eV. High-resolution spectra for individual elements were collected from 30 scans at 30 eV pass energy and 0.1 eV/step. For the XPS measurements, the powder samples were pressed onto indium foil. The spectra were acquired before and after the sample's surface was cleaned using an argon ion bombardment at 300 V. CasaXPS software (Casa Software Ltd., Teignmouth, UK) with Gaussian-Lorentzian product functions and a non-linear Shirley background subtraction was used to analyse the data and fit the curve (Ganea et al., 2022c).

2.4.7. Solid-State Nuclear Magnetic Resonance Spectroscopy (ss-NMR)

The solid-state ^{13}C and ^{15}N NMR spectra were recorded at 125.73 and 50.66 MHz Larmor frequencies using a Bruker Avance III 500 MHz wide-bore NMR spectrometer (Bruker, Billerica, MA, USA) operating at room temperature. The spectrometer contains a 4 mm double resonance (1H/X) MAS probe, and the material is packed in 4 mm zirconia rotors. The standard RAMP $^{13}C/^{15}N$ CP-MAS spectra were obtained under proton decoupling with TPPM, 2/4 ms contact periods, and spinning frequencies of 14/7 kHz. The acquisition parameters were optimized based on each sample investigated. The spectra were calibrated in relation to the CH_3 line in tetramethylsilane (TMS) and the $^{15}NO_2$ line in nitromethane using an indirect method. This procedure utilised L-Glycine as an external reference (C=O of glycine at 176.5 ppm for ^{13}C and −347.6 ppm for ^{15}N). Additionally, a line broadening of 20 Hz was applied to the ^{13}C spectra and 150 Hz to the ^{15}N spectra (Ganea et al., 2022c).

2.4.8. Brunauer-Emmett-Teller Analysis (BET)

The total surface area (St), pore volume (Vp), and pore radius (Rm) were determined using N_2 adsorption–desorption isotherms (recorded at −196°C). The BET technique was utilised for St, while for Vp and Rm, the Dollimore—Heal model was employed. The Sorptomatic 1990 device (Thermo Electron Corporation, Waltham, MA, USA) was used to record the isotherms. Physisorbed impurities were removed from the surface of the samples by degassing them for 5 h at 70°C and 1 Pa of pressure before determination.

2.4.9. Atomic Absorption Spectrometry (AAS)

The metals tested in the current thesis were: Cd, Cu, Cr, Fe, Mn, Ni, Pb, Zn. A ZEEnit 700 atomic absorption spectrometer (Analytik Jena, Germany) with a graphite furnace, an air-acetylene burner, and a single-element hollow cathode lamp was used to analyse the metal content. Five-points calibration curves were drawn for each investigated metal and dilutions were made for samples that had concentrations exceeding the calibration ranges. The reference material used for standards preparation (for the calibration curves) was 1000 mg L^{-1} Spectro Econ Chem Lab Stock

Solution (Chem Lab, Zedelgem, Belgium), and 1000 mg L^{-1} Merck Standard Solution (Merck KGaA, Darmstadt, Germany) was used for the quality control (Ganea et al., 2020).

2.4.10. Ultraviolet-Visible Spectroscopy (UV-VIS)

UV-Vis-NIR extinction spectra were acquired for the polymeric nanostructures using a Jasco V-670 UV−Vis−NIR spectrometer (JASCO Deutschland GmbH, Pfungstadt, Germany) at 1 nm spectral resolution, in 2 mm path length quartz cuvettes.

The dyes content was measured with a Jasco V-550 UV-VIS Spectrophotometer (JASCO Deutschland GmbH, Pfungstadt, Germany) equipped with a double-beam photometer and a single monochromator, was used to record UV-VIS spectra in the 190–900 nm wavelength range with a spectral resolution of 1 nm. Quartz cells of 10 mm length were utilized for the blank solution (distilled H_2O) and the samples. The dyes tested in this research were: crystal violet, tartrazine. Sample aliquots were collected both before and after performing the adsorption experiments, and the absorbance was measured at a 591 nm wavelength in the case of crystal violet, and at 421 nm for tartrazine.

2.4.11. Dynamic Light Scattering (DLS) and Zeta Potential Analysis

Particle size distribution (*via* Dynamic Light Scattering) and zeta-potential were measured in using the Zetasizer NanoZS90 (Malvern Panalytical Ltd, Malvern, UK). Analysis was performed at a scattering angle of 90 ° and a temperature of 22 °C. All experiments were performed in triplicate and the data are expressed as mean ± standard deviation (SD).

2.4.12. Physico-Chemical Parameters

Physico-chemical parameters of aqueous solutions (electrical conductivity—C, salinity, pH, oxidation-reduction potential—ORP, total dissolved solids—TDS) were measured with a Multi 350i multiparameter (WTW, Weilheim, Germany) (Ganea et al., 2020).

2.5. Batch Adsorption Experiments

2.5.1. Adsorption Assays

The batch sorption studies involved the preparation of stock solutions of different contaminant concentrations using ultrapure water produced with a Milli-Q (Millipore, Bedford, MA, USA). Two categories of pollutants were investigated in the current research:

- Inorganic Contaminants: heavy metals (Cu^{2+}, Zn^{2+}, Mn^{2+}, Pb^{2+}, Cd^{2+}, Cr^{3+}, Ni^{2+}, Fe^{3+})
- Organic Contaminants: synthetic dyes (crystal violet, tartrazine)

Adsorption experiments were completed at room temperature (25 °C) either in an HLC Heating-ThermoMixer MHR11 (DITABIS Digital Biomedical Imaging Systems AG, Pforzheim, Germany) or on magnetic stirring plates at a frequency of 600–700 rpm. Different parameters were analysed to study the effect on contaminant removal efficiency: initial contaminant concentration, interaction time and the pH of the contaminated solution (**Table 1**). The adsorbent materials were separated from the aqueous media magnetically (with a neodymium magnet) or via filtration (on Rotilabo folded filters, type 113 P, membrane Ø 150 mm, Macherey-Nagel GmbH, Dueren, Germany) or centrifugation (Loreena Centrifuge AFI-C300RF-E, SARL AFI Centrifuge, Château-Gontier-sur-Mayenne, France). The contaminant content in the supernatant was determined by AAS or UV-VIS measurements. The removal efficiencies and sorption capacities of the newly synthesized materials were calculated based on the next equations:

$$R\ (\%) = \frac{C_i - C_f}{C_i} \times 100$$

$$q\ (mg\ g^{-1}) = \frac{(C_i - C_f) \times V}{w}$$

where: R is the adsorption efficiency (%), Ci and Cf are the initial and final CV concentrations (mg L^{-1}), q is the sorption capacity (mg g^{-1}), V is the volume of solution (L), and w is the amount of adsorbent (g).

Table 1. Batch adsorption assays conditions (Ganea et al., 2020, Ganea et al., 2021, Ganea et al. 2022c))

Material	Contaminant Tested	Stock Solutions Concentrations	Volume of Stock Solution	Amount of Material Used	Contact Time	Material Separation Method
MNP@PAAA-NTA	Cu, Zn, Mn	2 different stock solutions/metal (40 and 100 mg L^{-1})	40 mL	800 mg	24 h	magnetic separation
MNP@PAAA-DA	Cu, Zn, Mn	6 different stock solutions/metal (10, 20, 40, 60, 80, 100 mg L^{-1})	25 mL	500 mg	24 h	magnetic separation
MNP@PAAA-FA	crystal violet	38 different stock solutions (0.45–500 mg L^{-1})	3 mL	10 mg	30 min	magnetic separation
ZD, ZT	Fe	5 different stock solutions/metal (5, 25, 50, 75, 100 mg L^{-1})	70 mL	300 mg	240 min	centrifugation

CHIT-PAAA	Pb, Cd	6 different stock solutions/metal (10, 20, 40, 60, 80, 100 mg L^{-1})	20 mL	400 mg	6 h	filtration
PAAA-*CL*-XLD	tartrazine	23 different stock solutions (1–500 mg L^{-1})	25 mL	500 mg	180 min	filtration
MMT-PBAAA-DA	Cu, Zn, Mn, Cd, Cr, Ni, Fe, Pb	2 different stock solutions/metal (40 and 100 mg L^{-1})	40 mL	800 mg	24 h	filtration
BPSD	tartrazine	3 different stock solutions (1 mg L^{-1}, 10 mg L^{-1} and 100 mg L^{-1})	50 mL	1000 mg	90 min	centrifugation
WRCG	crystal violet	6 different stock solutions (0.5 mg L^{-1}, 1 mg L^{-1}, 10 mg L^{-1}, 100 mg L^{-1}, 250 mg L^{-1} and 500 mg L^{-1})	30 mL	100 mg	180 min	centrifugation
WRSD	crystal violet	6 different stock solutions (0.5 mg L^{-1}, 1 mg L^{-1}, 10 mg L^{-1}, 100 mg L^{-1}, 250 mg L^{-1} and 500 mg L^{-1})	30 mL	100 mg	180 min	centrifugation

2.5.2. Adsorption Equilibrium Studies

A suitable theoretical expression that predicts the amount adsorbed and the solution concentration at equilibrium as a function of the operating variables (such as temperature, initial contaminant concentration, and adsorbent mass), is necessary for multistage adsorption computations. In the current research, the sorption equilibrium studies were performed on each synthesized material according to the criteria presented in **Table 2**. Experimental data were fitted on both the linear and non-linear forms of different isotherm models (Langmuir, Freundlich, Temkin, Dubinin-Radushkevich and Khan) (Ganea et al., 2021).

2.5.3. Adsorption kinetics

In order to completely describe the contaminant sorption mechanism onto the prepared materials, it was imperative to investigate the adsorption kinetics. In the current study, kinetic experiments were conducted on each synthesized material in accordance with the criteria outlined in **Table 3**. The experimental data were analyzed using both the linear and non-linear forms of the kinetic models (Ganea et al., 2021; Ganea et al., 2022c).

2.5.4. Material Recyclability Studies

Desorption experiments were performed to check the reusability of materials. Between 7-10 adsorption-desorption cycles were conducted in this regard on each material. Afterwards, the synthesized material was separated from the solution with an external magnetic, filtration or centrifugation. The materials were subsequently washed with 20 mL of 10% methanol solution of acetic acid and 5 mL absolute ethanol (in the case of dyes adsorption studies) and with 30 mL of 0.1 M HNO_3 solution and distilled water (for the heavy metals tests) (Ganea et al., 2021, Ganea et al., 2022c).

Table 2. Conditions used in the adsorption equilibrium studies performed (Ganea et al., 2021, Ganea et al. 2022c))

Material	Contaminant Tested	Stock Solutions Concentrations	Volume of Stock Solution	Amount of Material Used	Contact Time	Material Separation Method	Isotherm Model Used
MNP@PAAA-DA	Cu, Zn, Mn	6 different stock solutions/metal (10, 20,40, 60,80, 100 mg L^{-1})	25 mL	500 mg	24 h	magnetic separation	Langmuir Freundlich
MNP@PAAA-FA	crystal violet	38 different stock solutions (0.45–500 mg L^{-1})	3 mL	10 mg	30 min	magnetic separation	Langmuir Freundlich Dubinin-Radushkevich Temkin
CHIT-PAAA	Pb, Cd	6 different stock solutions/metal (10, 20, 40, 60, 80, 100 mg L^{-1})	40 mL	20 mg	24 h	filtration	Langmuir Freundlich Dubinin-Radushkevich Temkin Khan Redlich-Peterson Sips Toth Koble-Corrigan
MMT-PBAAA-DA	Pb	6 different stock solutions (10, 20, 40, 60, 80, 100 mg L^{-1})	40 mL	800 mg	240 min	filtration	Langmuir Freundlich

Table 3. Parameters considered for the kinetic sorption assays Ganea et al., 2021, Ganea et al. 2022c)

Material	Contaminant Tested	Stock Solutions Concentrations	Volume of Stock Solution	Amount of Material Used	Contact Times	Kinetic Model Used
MNP@PAAA-NTA	Cu, Zn, Mn	40 mg L^{-1}	60 mL	1.2 g	10 min 20 min 40 min 60 min 90 min	pseudo-first-order model
					120 min 180 min 240 min 300 min 360 min 480 min 600 min	pseudo-second-order model
MNP@PAAA-DA	Cu, Zn, Mn	25 mL	500 mg	25 mL	15 min 30 min	pseudo-first-order model
					45 min 60 min 90 min 120 min 150 min	pseudo-second-order model

					180 min 210 min 240 min	
MNP@PAAA-FA	crystal violet	0.50 mg L^{-1} 1 mg L^{-1} 10 mg L^{-1} 100 mg L^{-1} 250 mg L^{-1} 500 mg L^{-1}	30 mL	0.1 g	5 min 15 min 30 min 45 min 60 min 90 min 120 min 150 min 180 min	pseudo-first-order model pseudo-second-order model Weber-Morris intra-particle diffusion model
CHIT-PAAA	Pb, Cd	10 mg L^{-1} 20 mg L^{-1} 40 mg L^{-1} 60 mg L^{-1} 80 mg L^{-1} 100 mg L^{-1}	80 mL	0.04 g	1 min 5 min 10 min 20 min 30 min 45 min 1 h 3 h 6 h 9 h	pseudo-first-order model pseudo-second-order model Weber-Morris intra-particle diffusion model

					12 h 24 h	Elovich model
MMT-PBAAA-DA	Pb	40 mg L^{-1} 100 mg L^{-1}	40 mL	800 mg	10 min 30 min 60 min 90 min 120 min	pseudo-first-order model
					150 min 180 min 210 min 240 min 270 min 300 min	pseudo-second-order model
BPSD	tartrazine	3 different stock solutions (1 mg L^{-1}, 10 mg L^{-1} and 100 mg L^{-1})	50 mL	1000 mg	1 min 10 min 20 min 30 min	pseudo-first-order model
					40 min 50 min 60 min 90 min	pseudo-second-order model

WRCG	crystal violet	6 different stock solutions (0.5 mg L^{-1}, 1 mg L^{-1}, 10 mg L^{-1}, 100 mg L^{-1}, 250 mg L^{-1} and 500 mg L^{-1})	30 mL	100 mg	5 min 15 min 30 min 45 min 60 min 90 min 120 min 150 min 180 min	pseudo-first-order model pseudo-second-order model
WRSD	crystal violet	6 different stock solutions (0.5 mg L^{-1}, 1 mg L^{-1}, 10 mg L^{-1}, 100 mg L^{-1}, 250 mg L^{-1} and 500 mg L^{-1})	30 mL	100 mg	5 min 15 min 30 min 45 min 60 min 90 min 120 min 150 min 180 min	pseudo-first-order model pseudo-second-order model

2.5.5. Real-Life Contaminated Water Sampling

Several water samples were collected from two former mining areas in Romania (Roșia Montană and Novăț-Borșa) to test the adsorption efficiency of the synthesized materials on real-life contaminated aqueous solutions (**Figure 1**). These two sites were chosen since they are considered among the most polluted areas in Romania, with groundwaters, surface waters and soils having high concentrations of heavy metals reported. The water samples were collected in two seasons (summer and winter 2020) and were stored in 2L sterile polyethylene terephthalate bottles and kept in the fridge at 4°C until metal analysis and adsorption experiments were performed. The map with the sampling points was developed using ArcGIS 10.6.1 (ESRI, Redlands, CA, USA) (Ganea et al., 2022c).

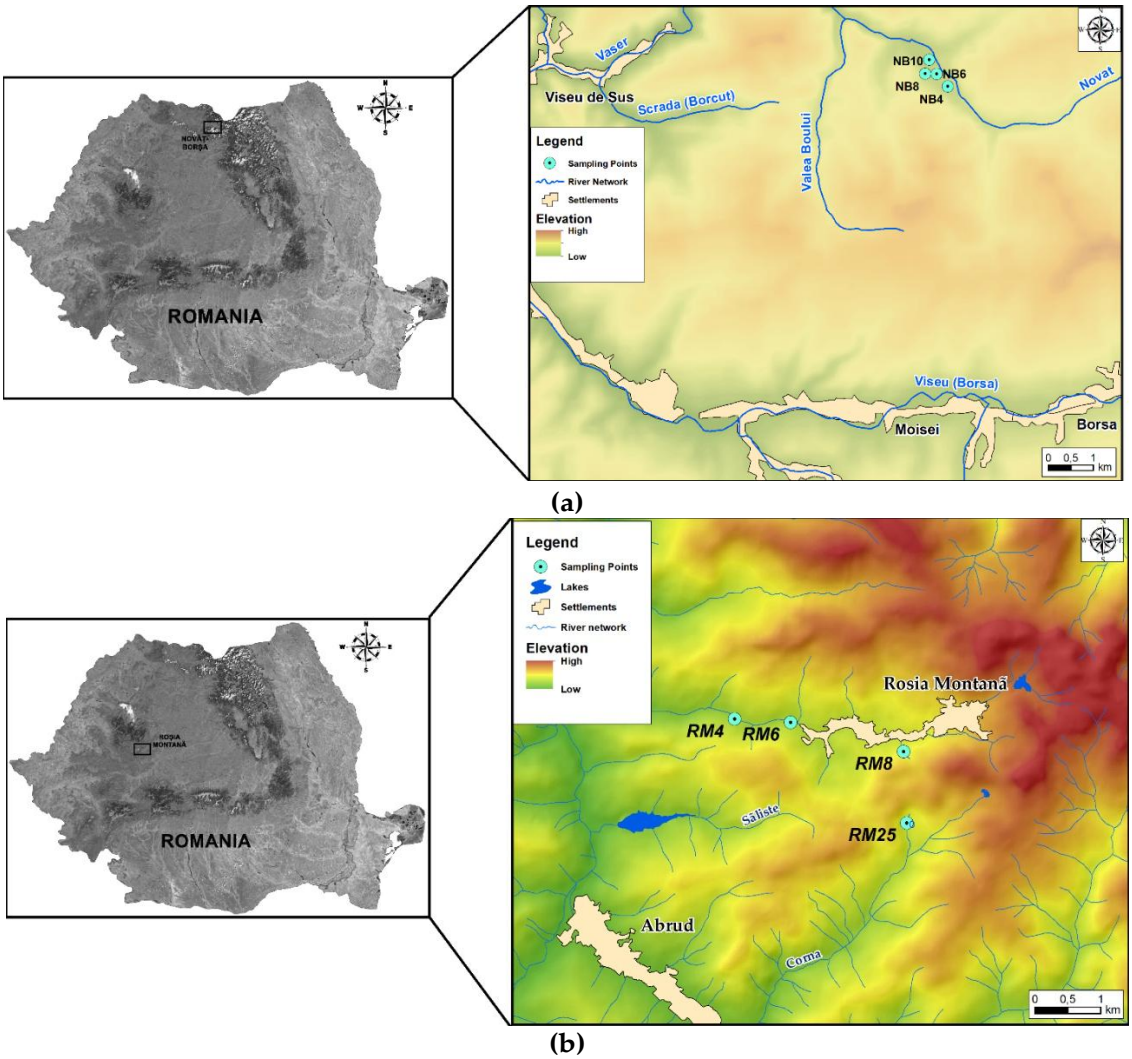

Figure 1. Map of the real-life contaminated water samples collected: **(a)** Novăț-Borșa Mining Area, **(b)** Roșia Montană Mining Area. (Ganea et al., 2022c)

2.5.6. 3D Adsorption Modelling

The 3D adsorption rate model is a representation that offers a comprehensive understanding of the adsorption process and the factors that affect the sorption capacities of materials (Roman et al., 2019). Contact time and initial contaminant concentration were identified as the primary parameters that influence the adsorption rates. The resolution of the 3D adsorption rate models was set as 1 mg L^{-1} (Ganea et al., 2021.

2.5.7. Statistical Analysis

Descriptive statistical analysis was performed using Origin v.2018 (OriginLab Corporation, Northampton, MA, USA). The least-square method and correlation coefficient (R^2) analysis were employed to evaluate the results of all equilibrium and kinetic models used in this study (Ganea et al., 2021). Apart from the above, Anscombe's quartet model was developed utilising Anaconda v.2–2.4.0 (numpy library) (Anaconda, Inc., Austin, TX, USA) and Python programming (Python v. 3.9.2, The Python Software Foundation, Beaverton, OR, USA).

2.5.8. Artificial Neural Networks Modelling

The adsorption process is challenging to model using only statistical approaches due to its high level of complexity. In the current study, three-layer ANNs (two inputs and one output) were constructed using The Neural Network Toolbox of MATLAB 9.5 (R2018b) mathematical software (MathWorks, Natick, MA, USA). These three layers were composed of two neurons in the input layer, which represented the initial contaminant concentration and the contact time, and one neuron in the output layer, which represented the amount of contaminant adsorbed. The algorithms used to learn the MLFFN comprised of 1000 iterations/material/contaminant and used linear transfer functions (purelin) and tangent sigmoid transfer functions (tan-sig). 80% of these data were used for training and 20% for testing/validating the algorithm (Ganea et al., 2022c).

3. EXPERIMENTAL RESULTS AND DISCUSSIONS

This chapter presents the detailed experimental results regarding the synthesis of the materials, their physicochemical characterization, and their performance in adsorption experiments aimed at removing pollutants, specifically heavy metals and organic dyes, from aqueous solutions.

3.1. Materials' Preparation and Characterization

The preparation and characterization of materials are critical steps in understanding their potential applications, particularly in the context of water treatment and environmental remediation. In this sub-chapter, the synthesis and detailed characterization of the various materials developed for the adsorption of pollutants from aqueous solutions. The synthesized materials have distinct properties as demonstrated through the various characterization techniques applied. Moreover, all these methods present significant information regarding the successful preparation of the materials. In the following sub-chapters, each of the ten materials prepared will be described, characterized and assessed in relation with the contaminants' adsorption performance.

3.1.1. Magnetic Nanostructures MNP@PAAA-NTA, MNP@PAAA-DA and MNP@PAAA-FA

❒ *Brief Description*

All three magnetic nanostructures developed appear as fine dark brown powders (**Figure 2**). The preparation procedures of **MNP@PAAA-NTA**, **MNP@PAAA-DA and MNP@PAAA-FA** are characterized by the next steps:

(i) synthesis of **PBAAA** by poly-Friedel-Crafts alkylation of *p*-hydroxymandelic acid

(ii) synthesis of **MNPs** by co-precipitation method

(iii) functionalization of **PBAAA** with **NTA/DA/FA** by opening the lactone rings in the polymer with the free amino groups

(iv) adsorption reaction of **PAAA-NTA/PAAA-DA/PAAA-FA** on the surface of the **MNPs**

(a) **(b)**

(c) **(d)**

Figure 2. Appearance of **PBAAA (a), MNP@PAAA-NTA (b)**, **MNP@PAAA-DA (c)** and **MNP@PAAA-FA (d)**

❒ *Infrared Spectroscopy (FTIR)*

A comparison of the infrared spectra of **MNP**, **PBAAA**, and **MNP@PAAA-NTA** is shown in **Figure 3**. It can be noticed that the magnetite (Fe_3O_4) absorption band at 580 cm^{-1} decreases in intensity in the spectrum of **MNP@PAAA-NTA**, highlighting the coating of **MNPs** with the polymer. The significant reduction of the bands located at 1734 cm^{-1} (carboxyl) and 1800 cm^{-1} (lactone) in the spectra of **MNP@PAAA-NTA** in comparison to the precursor **PBAAA** suggests that the **NTA** molecule has been attached to the polymer chain through the formation of an amide I bond (NH-C=O). Additionally, the FTIR spectra of **MNP@PAAA-NTA** shows an increase in the strength of the absorption band at 1635 cm^{-1} attributed to the amide group or to the negatively charged carboxyl group (Ganea, 2018; Ganea et al., 2020; Ganea et al., 2022b).

The same pattern was observed in the case of **MNP@PAAA-DA**, where the decrease in the intensity of the carboxyl and C=O absorption bands is an indicator of the amide formation via the lactone ring opening and the attachment of **DA** to the polymeric chain of **PBAAA** (Ganea, 2018; Ganea et al., 2022b).

In the FTIR spectrum of **MNP@PAAA-FA** the absorption band specific to the Fe-O bond appears to be split at 585 cm^{-1} and 631 cm^{-1}. The bands at 1608 cm^{-1} and 1646 cm^{-1} attributed to the N-H bending, N-C=O group and C=O bond (Amide I) are proof of the covalent attachment of **FA** to the polymeric chain. The aromatic hydrocarbons, which are abundant in the functionalised polymer's structure, exhibit absorption bands in the regions of 1400–1500 cm^{-1} and 1585–1610 cm^{-1} as a result of the C-C stretching vibrations present in the aromatic ring. The absorption band at 1297 cm^{-1} is associated with the C-O stretching bond, the one at 1187 cm^{-1} with the C-N bond, while the ones between 3147-3300 cm^{-1} can be attributed to the O-H, N-H and C-H stretching vibrations in the aromatic ring (Ganea et al., 2021).

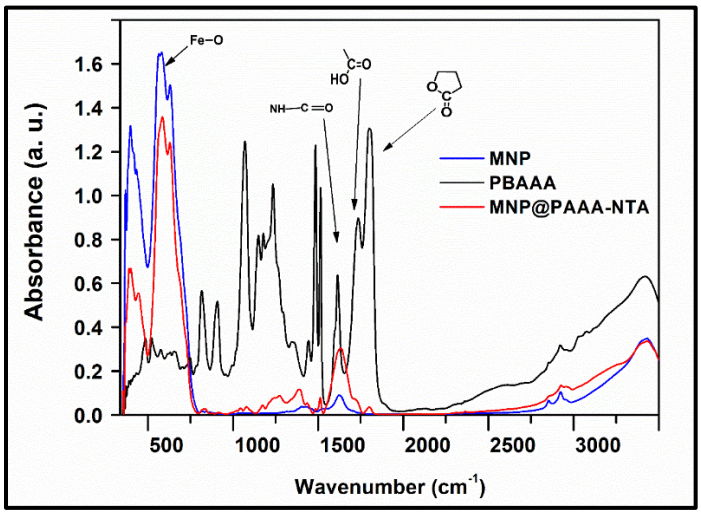

Figure 3. FTIR spectra of **MNP (blue line)**, **PBAAA (black line)** and **MNP@PAAA-NTA (red line)** measured between 400-4000 cm^{-1} (Ganea, 2018; Ganea et al., 2020; Ganea et al., 2022b)

❒ *Miscroscopic Analysis*

The magnetic nanostructures formed by the adsorption of **PBAAA** on the surface of the **MNPs** exhibit a core-shell architecture, with magnetite constituting the magnetic core and the functionalized **PBAAA** creating the organic shell. The magnetic nanostructures **MNP@PAAA-NTA** exhibit a relatively spherical morphology, with an average particle size of approximately 12-15 nm for **MNPs**, 16–22.2 nm for **MNP@PAAA-NTA** and **MNP@PAAA-DA**, and 20-27 nm for

MNP@PAAA-FA as depicted in **Figures 4 and 5** (Ganea, 2018; Ganea et al., 2020; Ganea et al., 2021; Ganea et al., 2022b).

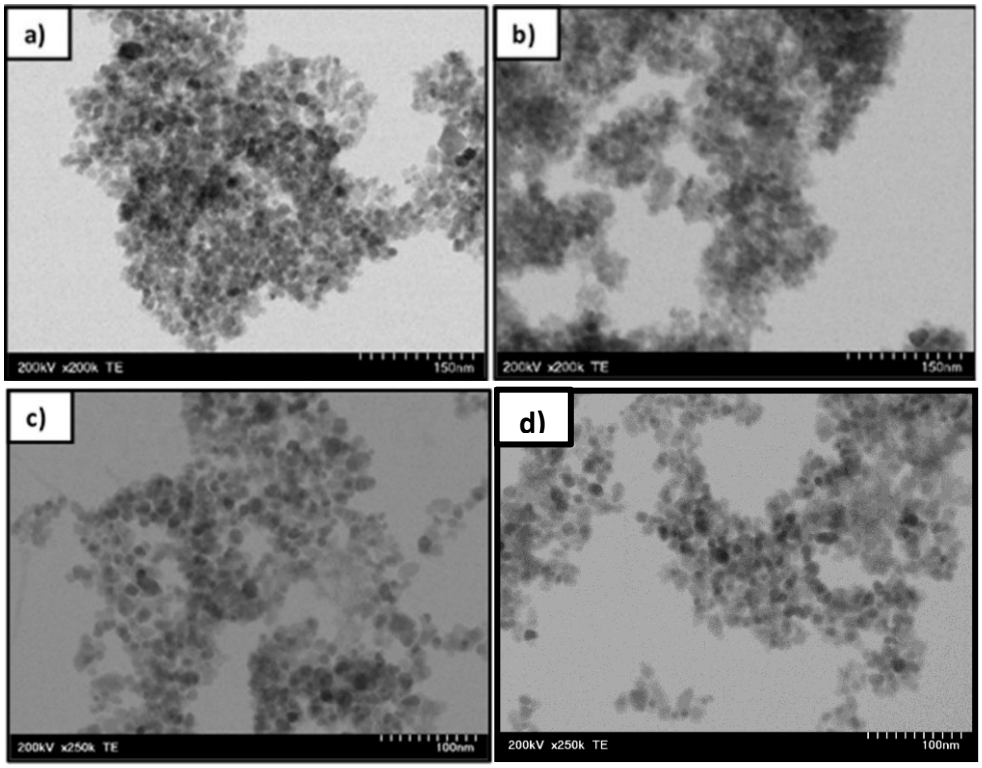

Figure 4. TEM images of **MNP (a)**, **MNP@PBAAA (b)**, **MNP@PAAA-NTA (c)**, and **MNP@PAAA-DA (d)** measured at an acceleration voltage of 200 kV using a 10 µl drop of a sample suspension dried on a copper grid and coated with a thin carbon film (Ganea, 2018; Ganea et al., 2020; Ganea et al., 2022b)

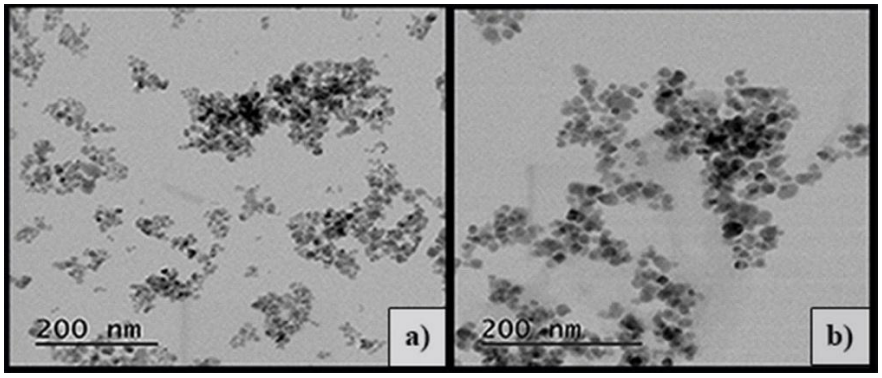

Figure 5. TEM images of **MNP (a)** and **MNP@PAAA-FA (b)** measured at an acceleration voltage of 200 kV using a 10 µl drop of a sample suspension dried on a copper grid and coated with a thin carbon film (Ganea et al., 2021)

❒ *Magnetization Measurements*

The saturation magnetization of **MNP**, **MNP@PAAA-NTA**, **MNP@PAAA-DA** and **MNP@PAAA-FA** was assessed to evaluate its suitability for magnetic separation (**Figure 6**). The decrease from 84 emu g^{-1} for **MNP** to 61 emu g^{-1} for **MNP@PAAA-NTA** and 67 emu g^{-1} for **MNP@PAAA-DA** is attributed to the addition of the functionalized polymer shell on the magnetite surface. In the case of **MNP@PAAA-FA**, the shape of the curve shows that the novel material exhibits a decrease in the saturation magnetization (to 58.70 emu g^{-1}) as a result of loading **MNPs** with the **PAAA-FA** coating, which increases the non-magnetic portion of the resultant nanomaterial (**Figure 7**). (Ganea, 2018; Ganea et al., 2020; Ganea et al., 2021; Ganea et al., 2022b).

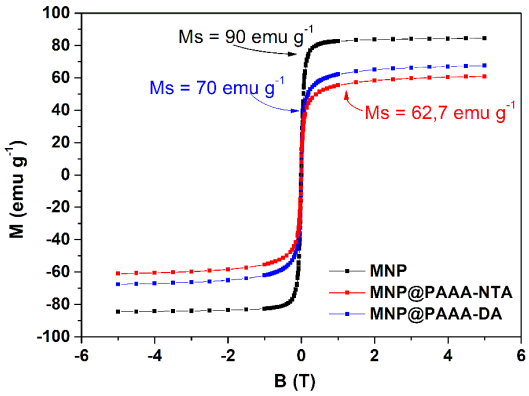

Figure 6. Magnetization vs. applied magnetic field for **MNP (black line), MNP@PAAA-NTA (red line)** and **MNP@PAAA-DA (blue line)** measured at room temperature (Ganea, 2018; Ganea et al., 2020; Ganea et al., 2022b)

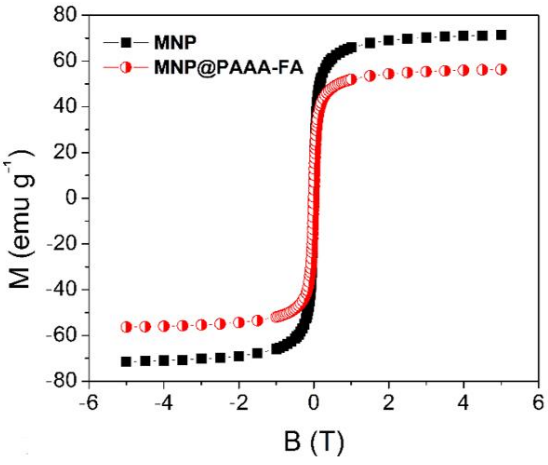

Figure 7. Magnetization vs. applied magnetic field for **MNP (black line)** and **MNP@PAAA-FA (red line)** measured at room temperature (Ganea et al., 2021)

3.1.2. Polymeric Nanostructures ZD and ZT

❒ *Brief Description*

Zein, the primary protein in corn endosperm, is abundant in proline and glutamine which contribute to its distinctive solubility profile. This is attributed to the amino acid sequence that contains more than half of the nonpolar units, such as proline, leucine, alanine, phenylalanine, isoleucine, valine, etc. In addition to its capacity to self-assemble into nanoparticles and its strong hydrophobic nature, zein is also biocompatible and biodegradable, being regarded as safe for human ingestion (Kacsó et al., 2018). Due to these characteristics, zein was successfully exploited in the development of novel polymeric nanostructures. These nanostructures have the aspect of a milky ivory solution as presented in **Figure 8**. The size, charge and functional groups of these new polymeric nanostructures recommend them for use in uptaking contaminants from wastewaters.

(a)

(b)

Figure 8. Images from the synthesis procedure of **ZD** and **ZT** nanoparticles **(a)** and their aspect after the completion of the preparation protocol **(b)**

❒ *Infrared Spectroscopy (FTIR)*

The FTIR spectra of the two types of nanoparticles **ZD** and **ZT** developed and their constituents, zein, DMAB and Tween 80. The zein spectrum includes the signals from the polysaccharides in gluten at 1061 cm^{-1} and 1130 cm^{-1}, the C=O stretching vibrations of the amide I band at 1651 cm^{-1}, the N-H bending vibration and C-N stretching vibration of the amide II band at 1235 cm^{-1} and 1530 cm^{-1}, and the O-H stretching band from carboxyl at 2930 cm^{-1} and 3360 cm^{-1}. The DMAB surfactant spectrum includes the bands typical for the C-N stretching vibration at 1100 cm−1 and the symmetric and asymmetric stretching and deformation vibrations of methylene at 1465 cm^{-1} and 2860 - 2918 cm^{-1}, respectively. Tween 80 spectrum presents the asymmetric C-O stretching vibration band at 1065 cm^{-1}, the H-O-H bending band at 1637 cm^{-1}, the C=O stretching band 1731 cm^{-1}, and the CH_2 and O-H stretching vibrations bands at 2934 cm^{-1}, and 3460 cm^{-1}, respectively. The FTIR spectra of the zein-based nanoparticles include signals both from zein and the surfactants used in the synthesis (sometimes with slight position shifts), demonstrating the successful completion of the preparation procedure.

❒ *Microscopic Analysis (TEM, SEM)*

The TEM analysis on the two types of zein-based nanoparticles revealed their spherical shape, with a similar size range (50-300 nm). ZD have a higher mean diameter than ZT (153 nm compared to 127 nm). SEM investigation showed that the zein has a relatively smooth surface, whereas **ZD** nanoparticles have pronounced cavities and **ZT** nanoparticles resemble a tree root network.

3.1.3. Modified Chitosan CHIT-PAAA

❒ *Brief Description*

The current research also investigated the potential to obtain a novel eco-friendly material, insoluble in water and readily separable by filtration, via an uncatalyzed process involving the cleavage of the lactone rings in the PBAAA polymer chain with the free amino groups of the chitosan. The copolymerization process yield for the **CHIT-PAAA** copolymer was 83%, while the grafting yield was 140%. The novel copolymer has the aspect of a granulated magenta powder and includes in his chemical structure carboxyl, lactones, phenols and amino groups able to bind

pollutant molecules from the environment (**Figure 9)** (Ganea, 2018; Ganea et al., 2022a; Ganea et al., 2022c).

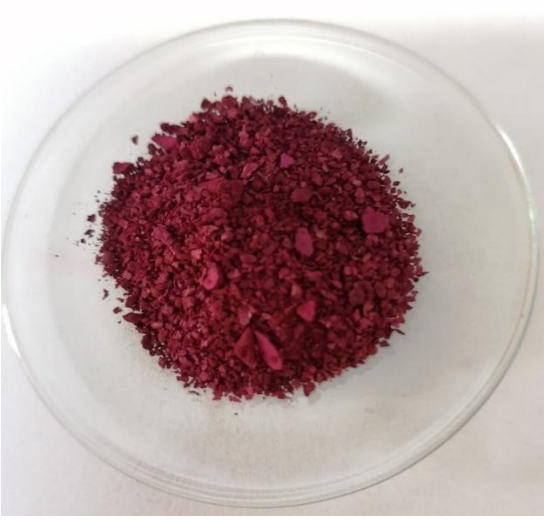

Figure 9. Aspect of the newly synthesized **CHIT-PAAA** copolymer

❒ *Solid State Nuclear Magnetic Resonance Spectroscopy (ss-NMR)*

The NMR spectra were recorded in solid state, specifically as ^{13}C ss-NMR and ^{15}N ss-NMR spectra, due to the fact that **CHIT-PAAA** is solid and insoluble in water or organic solvents. As illustrated in **Figure 10**, the ^{15}N ss-NMR spectrum of chitosan contains only one signal, while the final copolymer's spectrum contains two nitrogen atom signals. The peak at −374.4 ppm in the copolymer's spectrum belongs to the $-NH_2$ group of the chitosan chain, whereas the wide weaker peak at −259.5 ppm is ascribed to the newly formed amide bond (-NH-C=O), which emerges after the covalent attachment of chitosan to **PBAAA** through the opening of the lactone ring.(Ganea et al., 2022c)

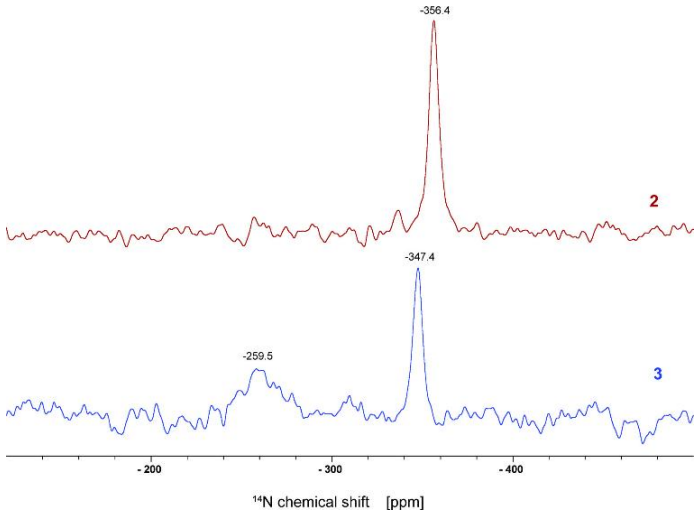

Figure 10. The ^{15}N ss-NMR spectra of the **CHIT (red line)** and **CHIT-PAAA (blue line)** (Ganea et al., 2022c)

The ^{13}C ss-NMR spectrum of the final copolymer exhibited substantial modifications in comparison to the initial materials (**Figure 11**). The attachment of chitosan to the **PBAAA** chain results in the absence of peaks about 50 ppm in the ^{13}C ss-NMR spectra of copolymer **CHIT-PAAA**, which are characteristic to the –CH in the lactone units from the ^{13}C ss-NMR spectra of **PBAAA** (Ganea et al., 2022c).

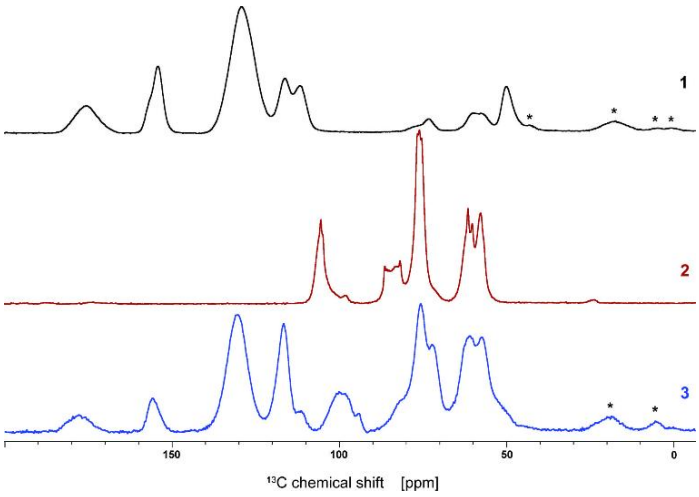

Figure 11. 13C ss-NMR spectra of **PBAAA (black)**, **CHIT (dark red)** and **CHIT-PAAA (blue)**. The asterisk indicates a sideband (Ganea et al., 2022c)

❒ *Microscopic Analysis (SEM)*

Figure 12 illustrates the significant morphological changes appearing after the modification of **CHIT** with **PBAAA**: the copolymer has the aspect of cauliflower-like aggregates, whereas its constituents have an arboreal structure (**PBAAA**) or a uniformly folded surface (**CHIT**). Thus, the rough, uneven surface of **CHIT-PAAA** with numerous apertures, recommends it for applications as adsorbent material (Ganea, 2018; Ganea et al., 2022a; Ganea et al., 2022c).

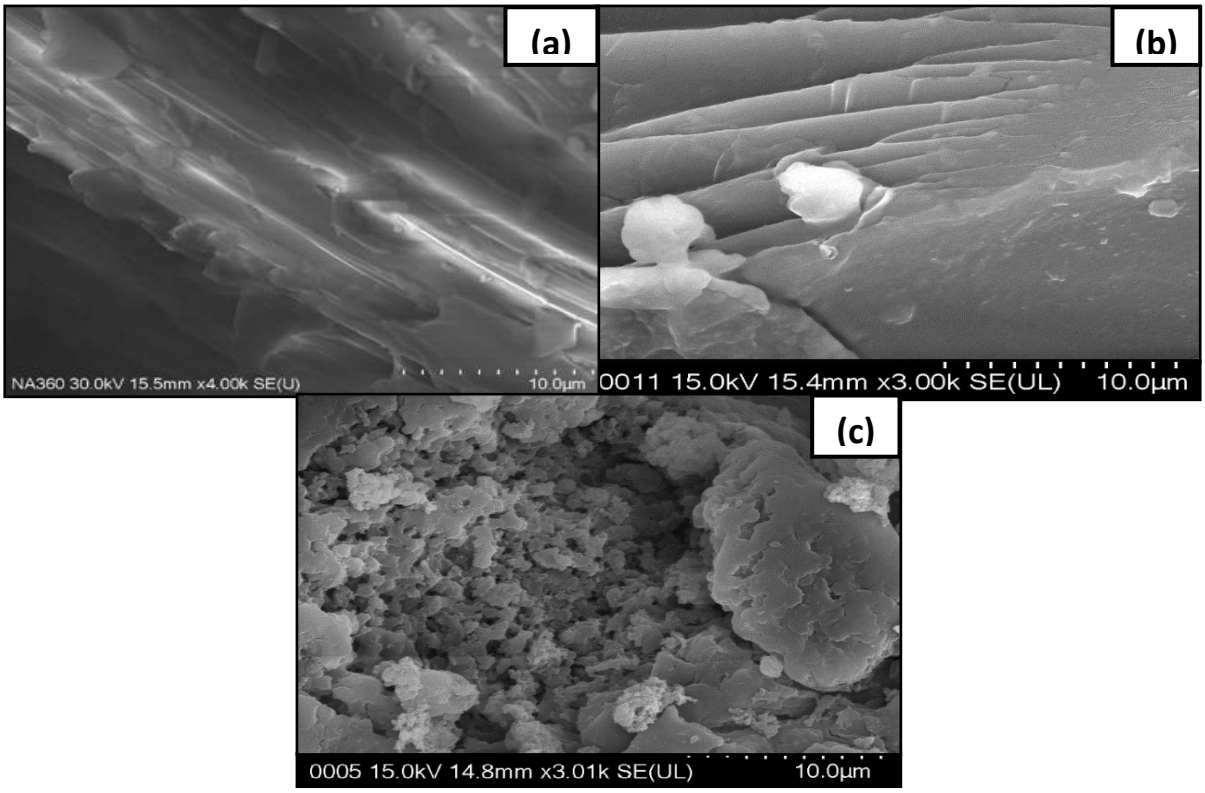

Figure 12. SEM images of **PBAAA (a)**, **CHIT (b)** and **PAAA-CHIT (c)** measured at an acceleration voltage of 15-30 kV using a 10 µl drop of a sample suspension dried on a copper grid and coated with a thin carbon film (Ganea, 2018; Ganea et al., 2022a; Ganea et al., 2022c)

3.1.4. Crosslinked Poly(benzofurane-co-arylacetic acid) PAAA-CL-XLD

❒ *Brief Description*

The presence of the lactone, carboxyl and hydroxy phenolic moieties in **PBAAA** facilitates extensive opportunities for derivatisation, including cross-linking with bifunctional reagents such as **XLD**. **PBAAA** can undergo crosslinking through the amide formation of the carboxyl and

lactone groups. The lactone group is the more reactive moiety and is already ring-opened. The carboxyl function can also generate amides under reflux, although being less reactive. Therefore, **PBAAA** chains can cross-link between two lactone rings, two carboxyl groups, or a lactone ring and a carboxyl group. The amide moieties that result are identical regardless of the functional groups from which they are generated (Nan et al., 2024). The resulting material **PAAA-*CL*-XLD** has the aspect of a dusty-pink color solid powder (**Figure 13**). Three sub-samples were prepared by varying the mass ratio between the polymer and the crosslinking agent as presented in **Table 4.**

Figure 13. Aspect of the newly synthesized polymer **PAAA-*CL*-XLD**

Table 4. PAAA-*CL*-XLD samples prepared

Sample	PBAAA : XLD Ratio
PAAA-*CL*_XLD_1	2 : 1
PAAA-*CL*-XLD_2	1 : 1
PAAA-*CL*-XLD_3	1 : 2

❒ *Solid State Nuclear Magnetic Resonance Spectroscopy (ss-NMR)*

Figure 14 illustrates the ^{13}C ss-NMR spectrum of **PAAA-*CL*-XLD**, which exhibits a signal at 44 ppm associated with the carbon atom of -CH_2-Ph- from the crosslinking agent **XLD**. Additionally, a decrease was noticed in the signal ascribed to the carbon -CH- atoms from the lactone ring of the polymer chain, appearing only as a shoulder at 50 ppm in the **PAAA-*CL*-XLD** spectrum. The 110–180 ppm region is characterized by the signals of the carbon atoms in the benzene rings, carboxylic and ester atoms, and the newly formed amide groups. It is important to note that the signal at 111 ppm, characteristic for benzofuranone, decreased, while the strength of the signal increased at 116 ppm (Nan et al., 2024).

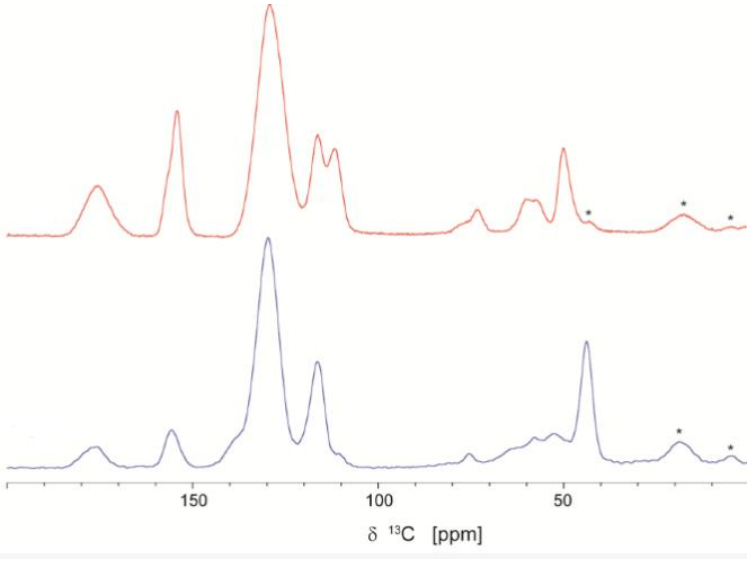

Figure 14. The ^{13}C ss-NMR spectra of **PBAAA (red line)** and **PAAA-*CL*-XLD (dark blue line)**. * indicates the sidebands (Nan et al., 2024)

The ^{15}N ss-NMR spectrum of **XLD** exhibited a signal at -370 ppm, which was significantly wider than the peak observed in the spectrum of **PAAA-*CL*-XLD** (**Figure 15**). Furthermore, this signal was moved to lower levels at −342 ppm (Nan et al., 2024).

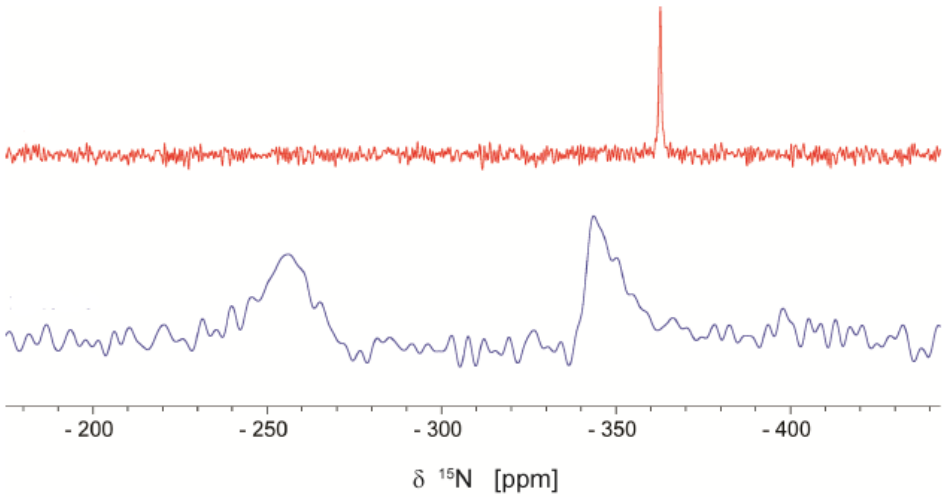

Figure 15. The ^{15}N ss-NMR spectra of **XLD (red line)** and **PAAA-*CL*-XLD (dark blue line)** (Nan et al., 2024)

3.1.5. Modified Montmorillonite MMT-PBAAA-DA

❒ *Brief Description*

The thermal polycondensation of *p*-hydroxymandelic acid was conducted as part of our initiative to create novel polymers that contain many functional groups. The process of modifying montmorillonite **MMT** with **PBAAA** functionalized with dopamine involved three steps: the synthesis of the **PBAAA** polymer via the Friedel-Crafts alkylation, the chelating reaction of **PBAAA** on **MMT**; and the covalent linkage of **DA** on the **PBAAA** chain (Ganea, 2018; Ganea et al., 2023a; Ganea et al., 2023b). The mineral-based polymer has the aspect of a dark pink powder as shown in **Figure 16**.

Figure 16. Appearance of the new mineral-based material **MMT-PBAAA-DA**

❒ *Thermogravimetric Analysis (TGA)*

Figure 17 displays the TGA thermograms of **MMT**, **PBAAA**, and **MMT-PBAAA-DA** measured from ambient temperature to 800 °C. The elimination of interlayer water between the silicate sheets of **MMT** counts for the 6% mass loss observed from around 40-122 °C. The interlayer cation influences both the total quantity of water discharged and the process's temperature. The loss of structural water due to the dehydroxylation of the **MMT** layers causes a 4% weight loss between 200-800 °C. The TGA curve of the novel material **MMT-PBAAA-DA** exhibits a cumulative weight reduction of 21% in two phases: the first one between 40-90 °C (6% weight loss) and the second one from 350 °C to 800 °C (15% weight loss). This last value is 11% greater than **MMT**, serving as evidence for the **PBAAA-DA** coating (Ganea, 2018; Ganea et al., 2023a; Ganea et al., 2023b).

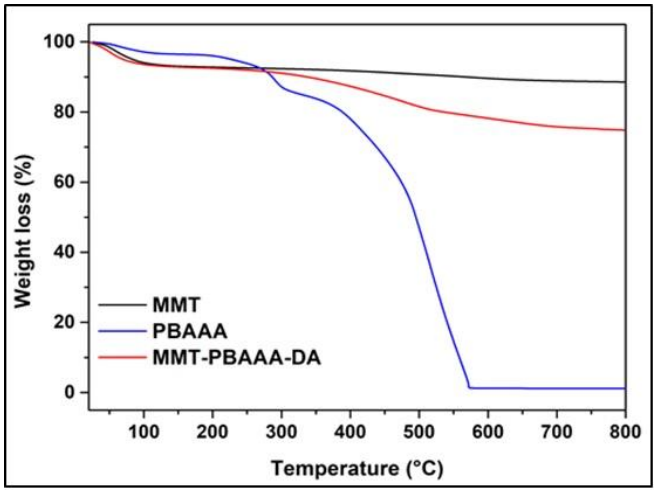

Figure 17. TGA analysis of **MMT (black line), PBAAA (blue line)** and **MMT-PBAAA-DA (red line)** performed in air from 30 °C to 800 °C with a heating rate of 10 °C min^{-1} (Ganea, 2018; Ganea et al., 2023a; Ganea et al., 2023b)

3.1.6. Composite Based on Banana Peel and Stone Dust (BPSD)

❒ *Brief Description*

This composite material promotes sustainability and circular economy since is prepared by combining two types of wastes widely spread in the environment as a result of the activities in the extractive and construction materials processing industry (stone dust) and food/daily consumption (banana peels). This material has the aspect of brown-coloured friable aggregates as presented in **Figure 18**. Due to its porous structure and the chemical properties of its components, this material has the ability to adsorb and retain various pollutants such as heavy metals or persistent organic compounds from the environment (Ganea & Nan, 2023b).

Figure 18. Appearance of the stone dust **SD (left)** constituent and the synthesized composite **BPSD (right)** (Ganea & Nan, 2023b)

3. EXPERIMENTAL RESULTS AND DISCUSSIONS

❒ *Microscopic Analysis (SEM-EDX)*

The EDX elemental distribution of stone dust emphasizes the presence of K, Si, Al in a high proportion, Fe and O in a lower proportion, whereas the carbon atom is in a negligible amount (**Figure 19**). On the other hand, the elemental distribution of the resulting material **BPSD** indicates a larger proportion of the carbon atom. This distribution is mainly due to the complex mineralogical structure of the stone dust.

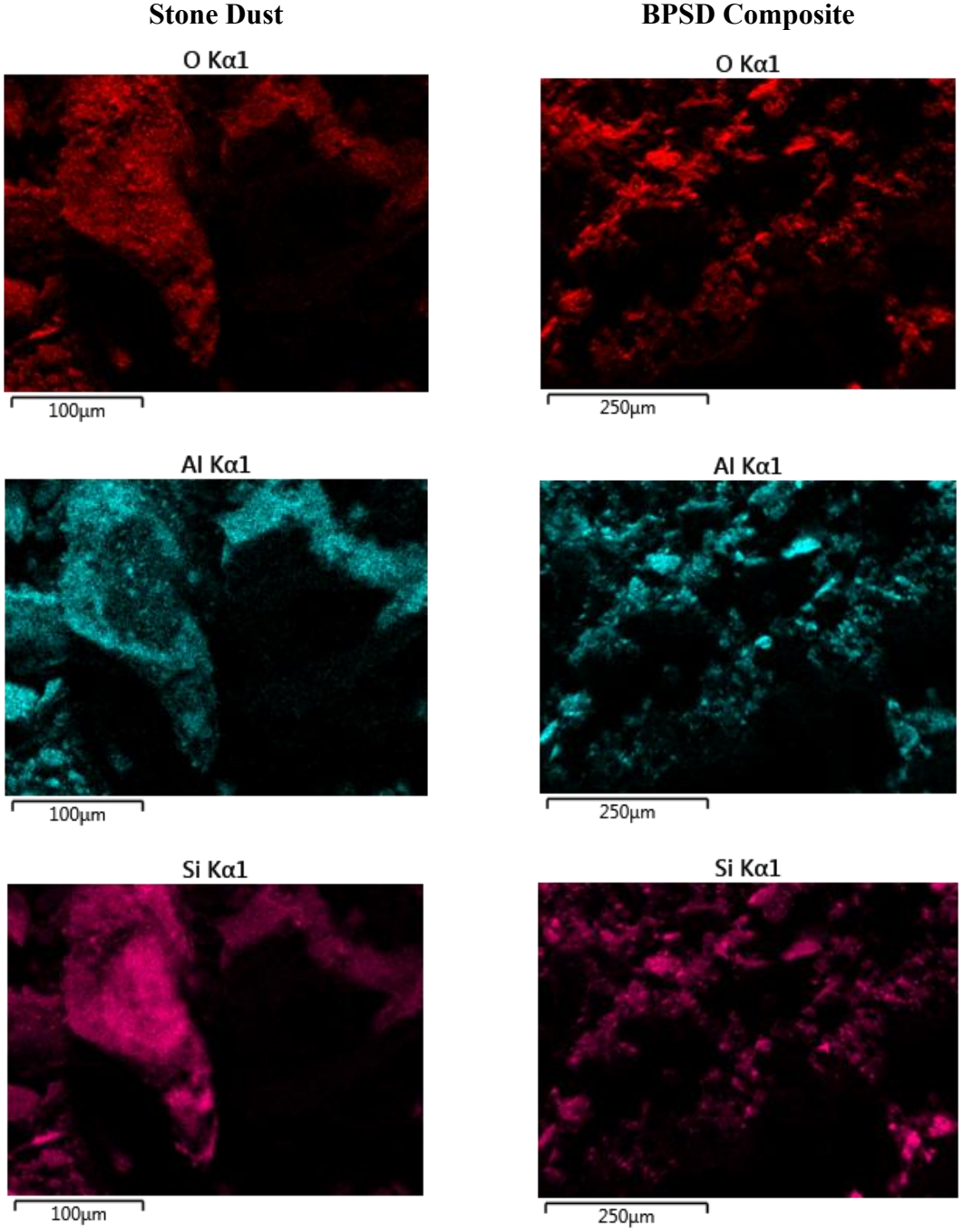

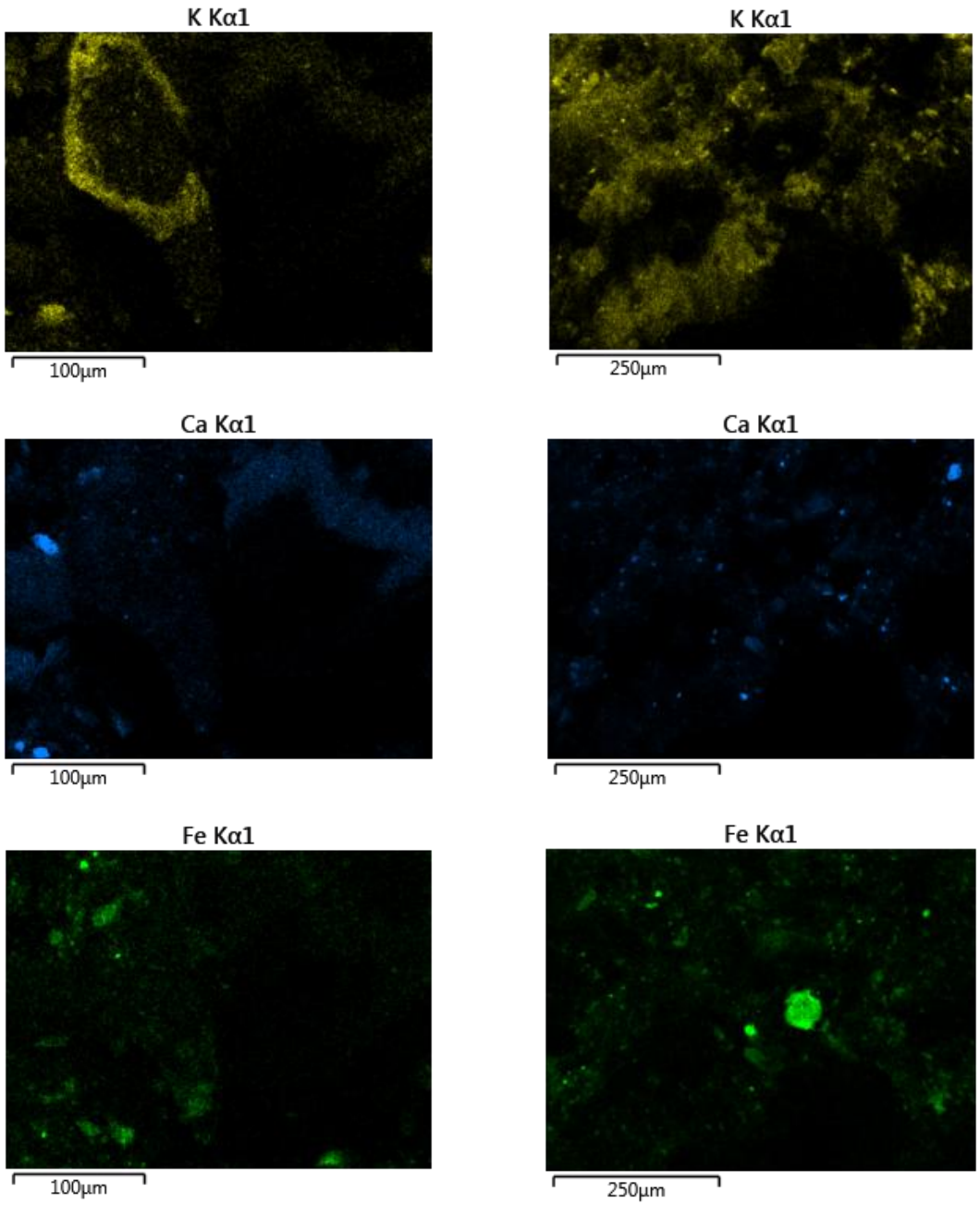

Figure 19. EDX mapping of stone dust **SD (left column)** and the **BPSD** waste-based composite **(right column)** (Ganea & Nan, 2023b)

3.1.7. Composite Based on Watermelon Rind and Coffee Grounds (WRCG)

❒ *Brief Description*

The sustainable composite **WRCG** was obtained by thermally treating the mixture of two

organic wastes (watermelon rind **WR** and coffee grounds **CG**) generated in large quantities from daily household consumption activities or from the food and HoReCa industry. The porous watermelon rinds are rich in organic compounds such as pectin, cellulose, proteins, carotenoids and citrulline, whereas coffee grounds contain numerous amino acids, polyphenols and polysaccharides in the structure. The heat treatment of the watermelon rinds and the coffee grounds used to obtain the new composite facilitated the activation of functional groups that promote the binding of contaminants from wastewater. The resulting material **WRCG** consists of small, porous, friable, brown coloured aggregates (**Figure 20**) (Ganea & Nan, 2024).

Figure 20. Appearance of the **WRCG** composite (Ganea & Nan, 2024)

❒ *Microscopic Analysis (SEM-EDX)*

The EDX spectra of the watermelon rinds **WR**, coffee grounds **CG** and the resulting composites **WRCG 1:1** and **WRCG 4:1** can be seen in **Figure 21**. **WRCG 1:1** composite includes in its structure C and O in a large proportion (68.8% and 30.3%, respectively) and K, Ca, Mg, Cu, Zn in smaller amounts (0.1-0.5%). In contrast, the elemental distribution of **WRCG 4:1** composite shows a slightly higher input of the C atom (73.4%) and lower proportions of the other elements (O - 26.2%, K - 0.2%, Cu - 0.1%, Mg - 0.1%) (Ganea & Nan, 2024).

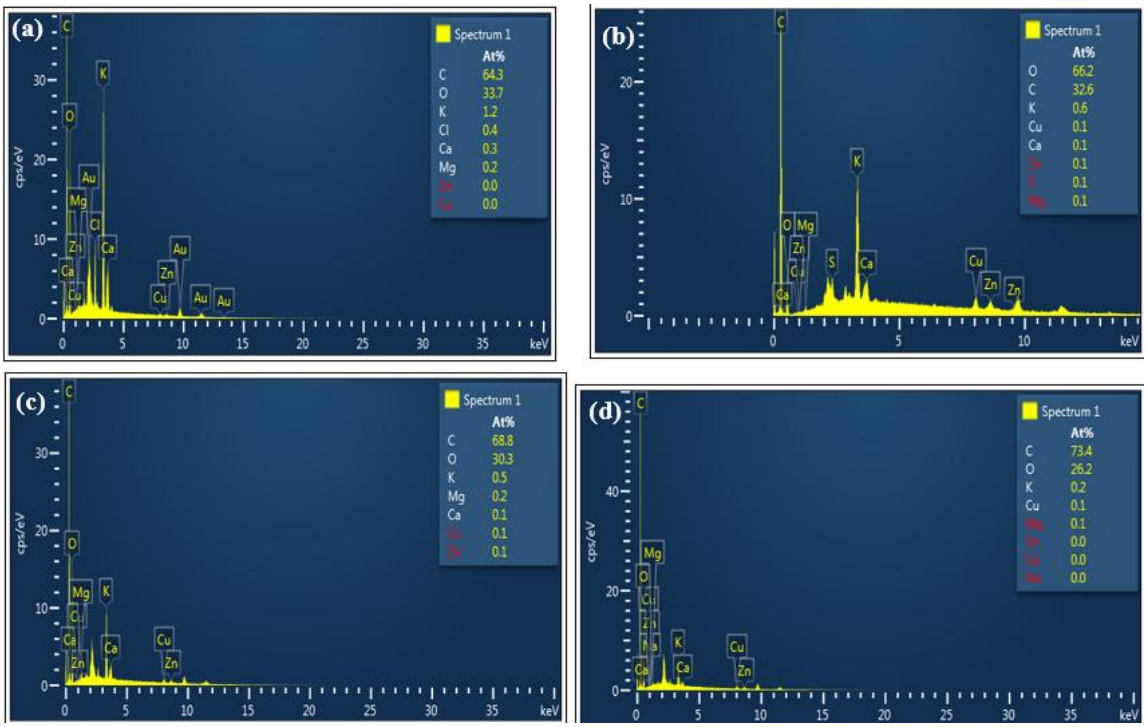

Figure 21. EDX spectra of **WR (a)**, **CG (b)** and the waste-based composites **WRCG 1:1 (c)** and **WRCG 4:1 (d)** (Ganea & Nan, 2024)

3.1.8. Composite Based on Watermelon Rind and Stone Dust (WRSD)

❒ *Brief Description*

WRSD is an environmentally-friendly composite obtained by combining stone dust **SD** (an inorganic waste generated in the extractive and construction materials industry) and watermelon rinds **WR** (organic waste resulting from daily consumption and food sector). The material has the aspect of brown and grey aggregates as presented in **Figure 22**.

Figure 22. The appearance of **WRSD** waste-based composite

❒ *Microscopic Analysis (SEM-EDX)*

The EDX spectra indicate that **WRSD 1:1** composite includes in its structure O in a high proportion (51.6%) and C in a lower amount (31%) (**Figure 26**). In contrast, **WRSD 4:1** composite has C in a higher content (47.8%) and less O (42%), reflecting the different compositions used in their synthesis. The composites contain also other elements in lower proportions such as: Si (8.5% in the case of **WRSD 1:1** and 5.2% in **WRSD 4:1**), Al (3.2% in **WRSD 1:1** and 1.8% in **WRSD 4:1**), Na (1.6% in **WRSD 1:1** and 0.9% in **WRSD 4:1**), Fe (1.3% in **WRSD 1:1** and 0.6% in **WRSD 4:1**), Mg (1.1% in **WRSD 1:1** and 0.7% in **WRSD 4:1**).

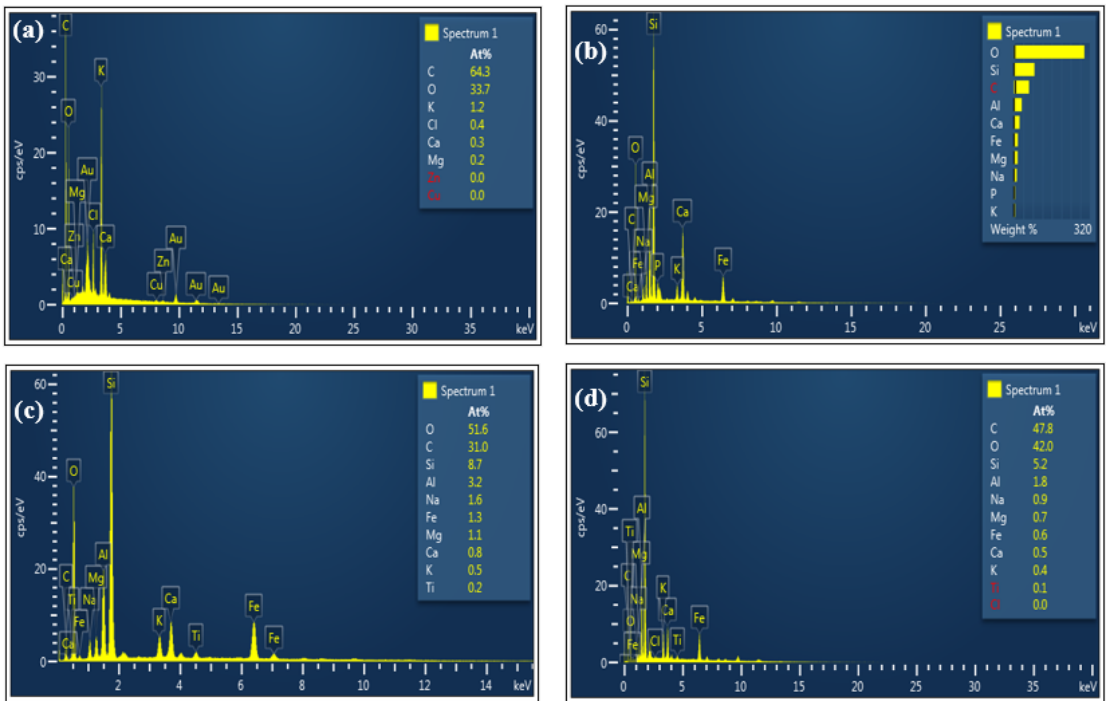

Figure 23. The EDX spectra of **WR (a)**, **SD (b)** and the waste-based composites **WRSD 1:1 (c)** and **WRSD 4:1 (d)**

3.2. Batch Adsorption Experiments

This sub-chapter presents the results of the adsorption tests conducted on the four categories of materials previously synthesized and characterized.

3.2.1. Experiments on Stock Solutions

*3.2.1.1. Magnetic Nanostructures **MNP@PAAA-NTA***

The following results of the batch adsorption experiments on **MNP@PAAA-NTA** have been previously published in the scientific literature (Ganea et al., 2021). **MNP@PAAA-NTA**'s removal efficiency and sorption capacity were examined in relation to two distinct beginning heavy metal concentrations (40 mg L^{-1} and 100 mg L^{-1}). **Figure 24a** illustrates the adsorption efficiency for Cu (pH = 4.24), Zn (pH = 4.77) and Mn (pH = 4.83) stock solutions. At higher metal concentrations, the removal efficiency displays a decreasing trend: Cu (5.00% at 40 mg L^{-1} and 0.16% at 100 mg L^{-1}), Zn (40.22% at 40 mg L^{-1} and 1.17% at 100 mg L^{-1}), and Mn (2.18% at 40 mg L^{-1} and 1.34% at 100 mg L^{-1}). The sorption capacity of **MNP@PAAA-NTA** determined in the batch studies on stock solutions are displayed in **Figure 24b**, emphasising the following metal affinity: Zn > Mn > Cu. The sorption capacity tendency exhibits a similar decrease as the initial concentrations increase:Cu (0.11 mg g^{-1} at 40 mg L^{-1} and 0.01 mg g^{-1} at 100 mg L^{-1}) and Zn (0.81 mg g^{-1} at 40 mg L^{-1} and 0.06 mg g^{-1} at 100 mg L^{-1}). Conversely, the adsorption capacity of **MNP@PAAA-NTA** for Mn experienced a slight increase from 0.04 mg g^{-1} at 40 mg L^{-1} to 0.07 mg g^{-1} at 100 mg L^{-1}. It is anticipated that the relatively low removal efficiencies and sorption capacities, can be enhanced by reducing the pH and utilizing a higher dosage of the sorbent **MNP@PAAA-NTA.**

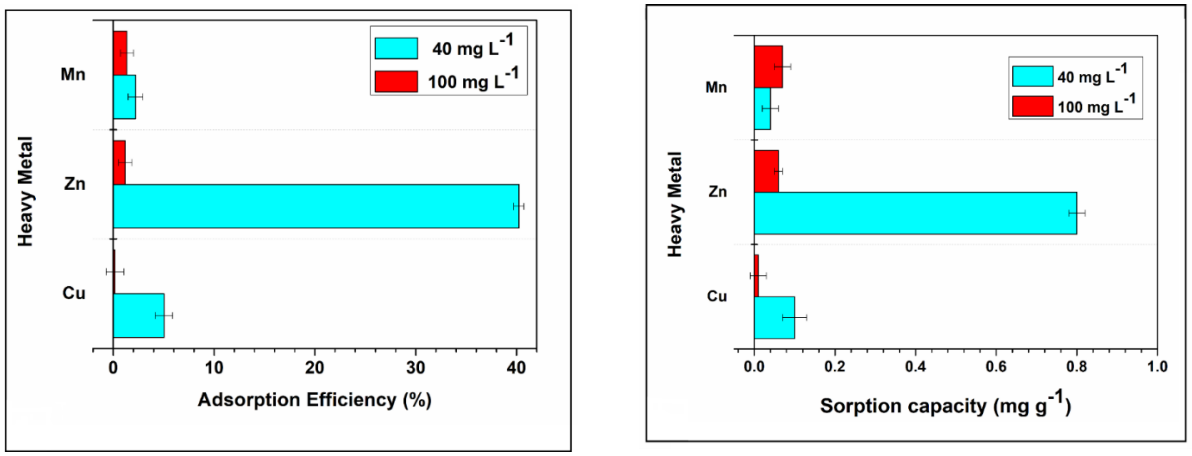

(a) **(b)**

Figure 24. The effect of initial metal concentration on **(a)** the adsorption efficiency and **(b)** sorption capacity of **MNP@PAAA-NTA.** (Ganea et al., 2020).

*3.2.1.2. Magnetic Nanostructures **MNP@PAAA-DA***

MNP@PAAA-DA magnetic nanostructures were tested for the adsorption of Cu, Mn and Zn at different concentrations in stock solutions. Overall, the efficiency of **MNP@PAAA-DA** was relatively low, except at 40 mg L^{-1} when it reached the maximum of 62.26% **(Figure 25)**. As it can be seen in, at low and medium concentrations (10−60 mg L^{-1}), the newly synthesized material presented higher removal efficiencies and sorption capacities for Cu (14.75−62.26% and 0.11−2.04 mg g^{-1}) as compared to the other metals investigated (1.74−28.09% and 0.014–0.032 mg g^{-1} for Mn; 1.77−20.89% and 0.01−0.14 mg g^{-1} for Zn). However, at higher concentrations (80 mg L^{-1} and 100 mg L^{-1}), the magnetic nanostructures registered a slightly better adsorption efficiency and sorption capacity for Mn (24.90−28.09 mg L^{-1} and 1−1.4 mg g^{-1}, respectively).

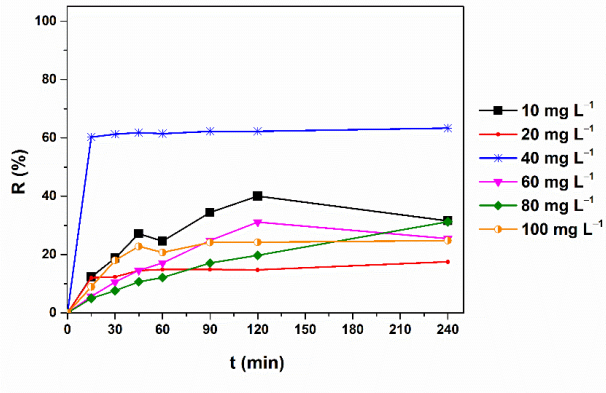

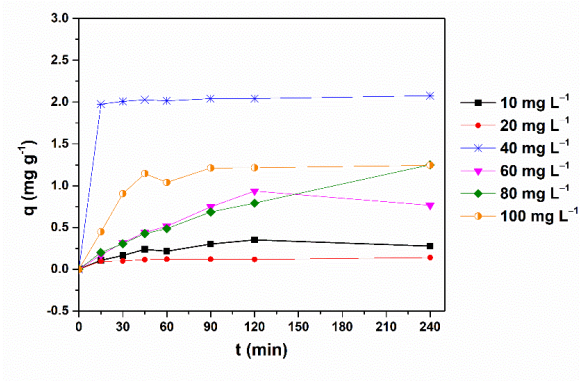

Cu

(a) **(d)**

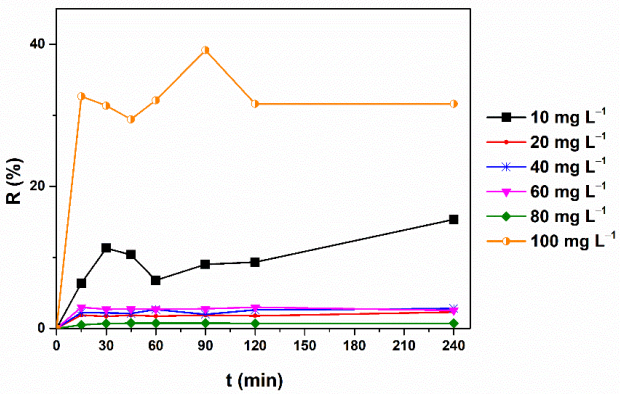

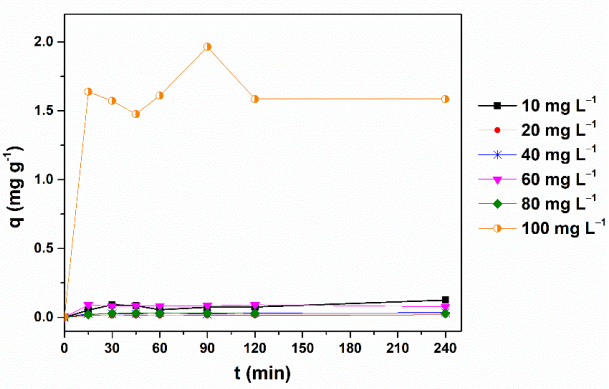

Mn

(b) **(e)**

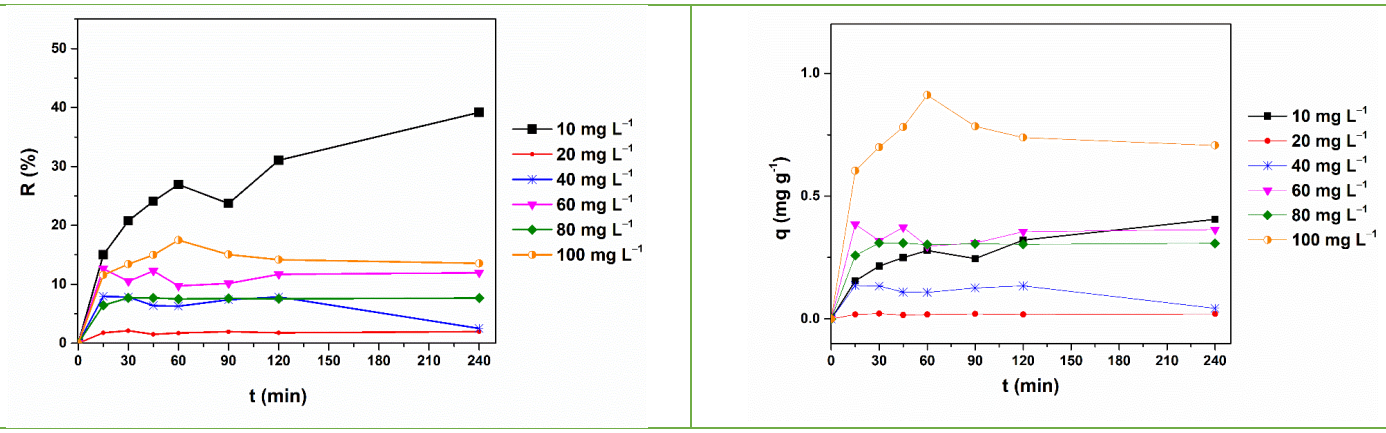

Zn

(c) **(f)**

Figure 25. The effect of contact time on the Cu, Mn and Zn removal efficiency **(a–c)** and sorption capacity **(d–f)** of **MNP@PAAA-DA**

*3.2.1.3. Magnetic Nanostructures **MNP@PAAA-FA***

The following results regarding the adsorption experiments on these new magnetic nanostructures were previously reported in the literature (Ganea et al., 2021). The adsorption capacity/removal efficacy of **MNP@PAAA-FA** was examined in relation to the initial crystal violet concentrations (**Figure 26**). The initial dye concentrations from 0.45–500 mg L^{-1} resulted in extremely high removal efficiencies (82.29%–92.44%). However, these efficiencies experienced a linear decline to 38.91% at 200 mg L^{-1} and were approaching the saturation limit at 500 mg L^{-1} (12.11%).

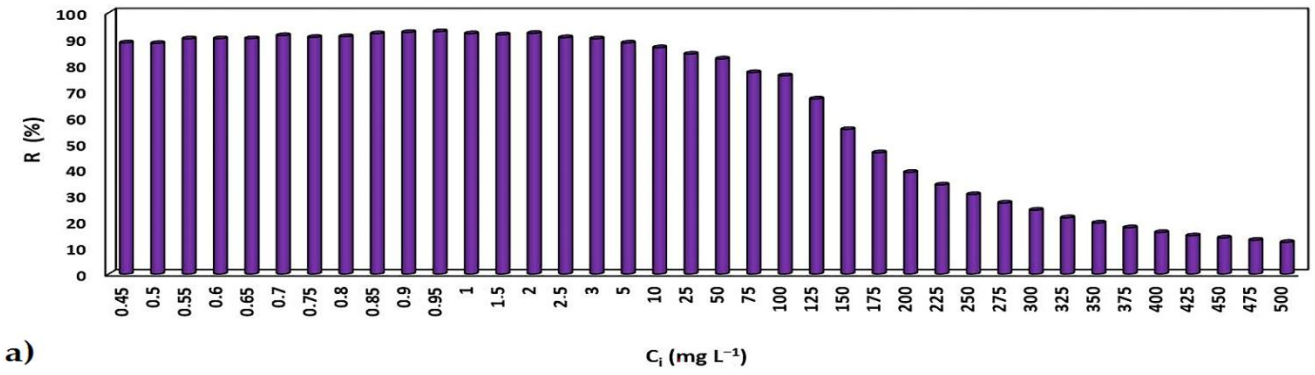

a)

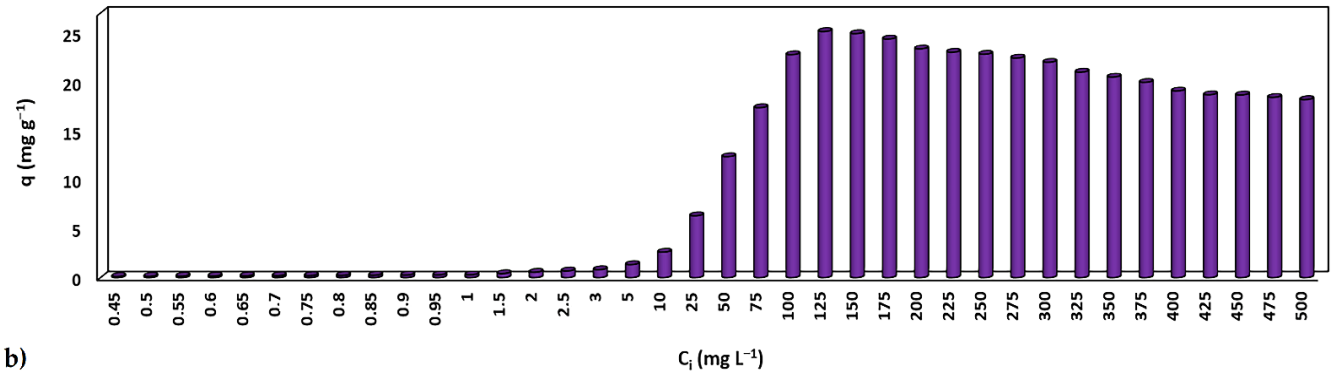

Figure 26. Effect of initial CV concentrations (0.45–500 mg L^{-1}) on the removal efficiency **(a)** and adsorption capacity **(b)** of **MNP@PAAA-FA** determined by UV-VIS spectroscopy at a spectral resolution of 1 nm and 591 nm wavelength (Ganea et al., 2021).

The reusability of **MNP@PAAA-FA** was also investigated. **Figure 27** illustrates the exceptional CV adsorption efficiency of **MNP@PAAA-FA** upon completion of 10 cycles of adsorption-desorption. The removal efficiency experienced a gradual decline from 100% to 97.63% during the initial five cycles, ultimately settling at a minimum of 88.74% following the tenth regeneration stage.

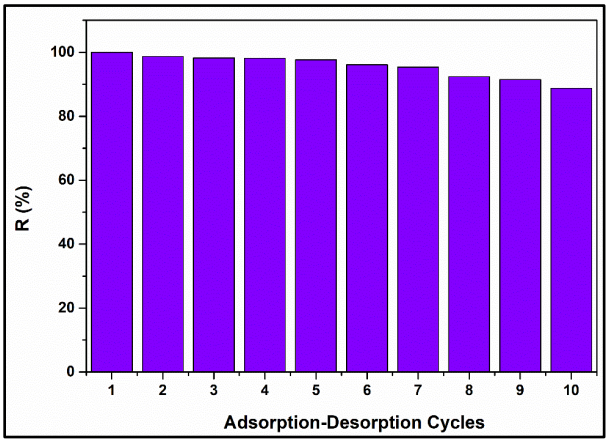

Figure 27. Reusability of **MNP@PAAA-FA** after conducting 10 cycles of adsorption-desorption (Ganea et al., 2021).

*3.2.1.4. Polymeric Nanostructures **ZD** and **ZT***

Preliminary metal adsorption studies were conducted on **ZD**, **ZT** and **zein**. Other investigations are undergoing in order to completely characterize the sorption behaviour of these

polymeric nanostructures for heavy metals. As it can be noticed in **Figure 28**, zein had the highest adsorption efficiencies (90% and 35%, respectively) at 5 and 25 mg L^{-1} Fe, while at 50 mg^{-1} Fe **ZT** and **zein** performed the best, reaching an efficiency of 50%. **ZT** recorded Fe retention efficiencies of over 60% at concentrations of 75 and 100 mg^{-1} Fe, while **ZD** had 40% efficiency.

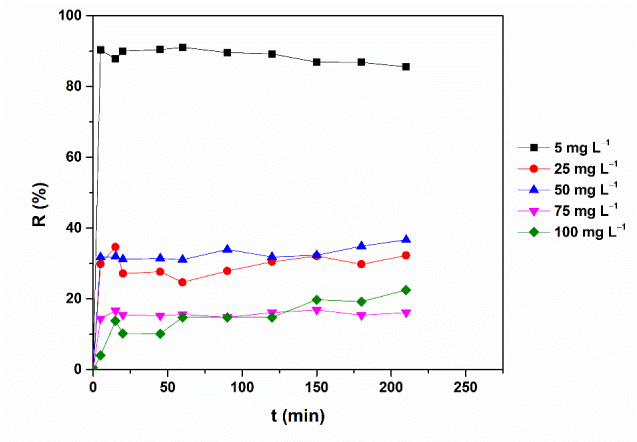

(a)

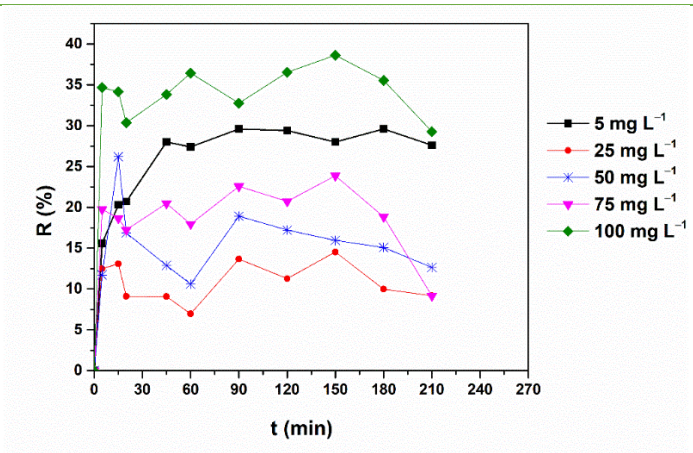

(b)

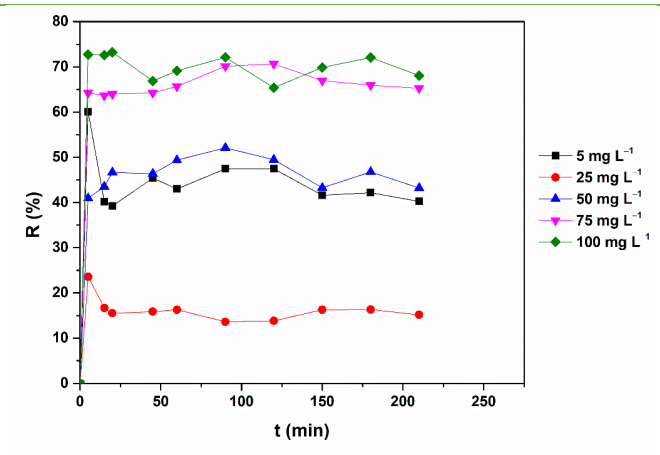

(c)

Figure 28. Effect of contact time on the Fe removal efficiency of zein **(a)** and ZD **(b)** and ZT **(c)** nanostructures

*3.2.1.5. Modified Chitosan **CHIT-PAAA***

The next results on the adsorption experiments performed with **CHIT-PAAA** were previously reported in the scientific literature (Ganea et al., 2022c). The initial phase of the experiments on stock solutions involved the impact examination of the contact time and the initial concentrations of Pb and Cd on the adsorption efficiency/sorption capacity of **CHIT-PAAA**. Pb demonstrated extremely high removal efficiency (90.63–96.07%) over a range of metal concentrations between 10 and 60 mg L^{-1}, as shown in **Figure 29a**. However, a declining trend (76.71–84.60%) is observed at high values (80–100 mg L^{-1}). Cd exhibited superior adsorption efficiencies (62.20%–68.60%) at lower concentrations compared to those achieved at higher values. As anticipated, the sorption capacity increased in proportionally with the metal concentration, with maximum values of 153.42 mg g^{-1} and 102.26 mg g^{-1} for Pb and Cd at 100 mg L^{-1}, respectively (**Figure 29b**).

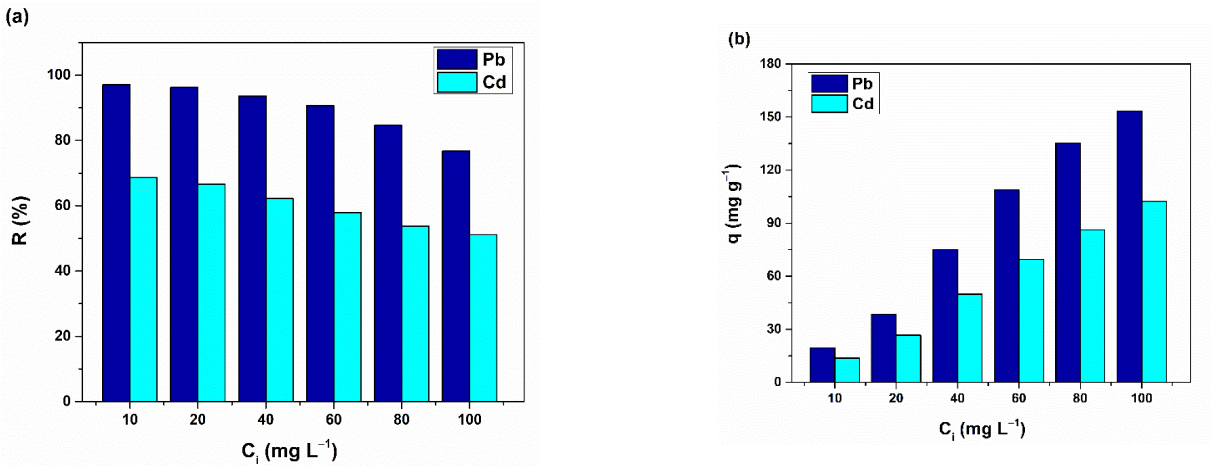

Figure 29. Removal efficiency **(a)** and sorption capacity **(b)** of **CHIT-PAAA** on Pb and Cd stock solutions (Ganea et al., 2022c)

The impact of contact time on the development of Pb and Cd adsorption onto **CHIT-PAAA** is depicted in **Figure 30**. Fast adsorption was observed in the initial hour of interaction with the novel material for both metals that were examined. After 45 minutes of contact time for Pb and 60 minutes for Cd, the maximum adsorption efficiency was recorded, and equilibrium was then achieved.

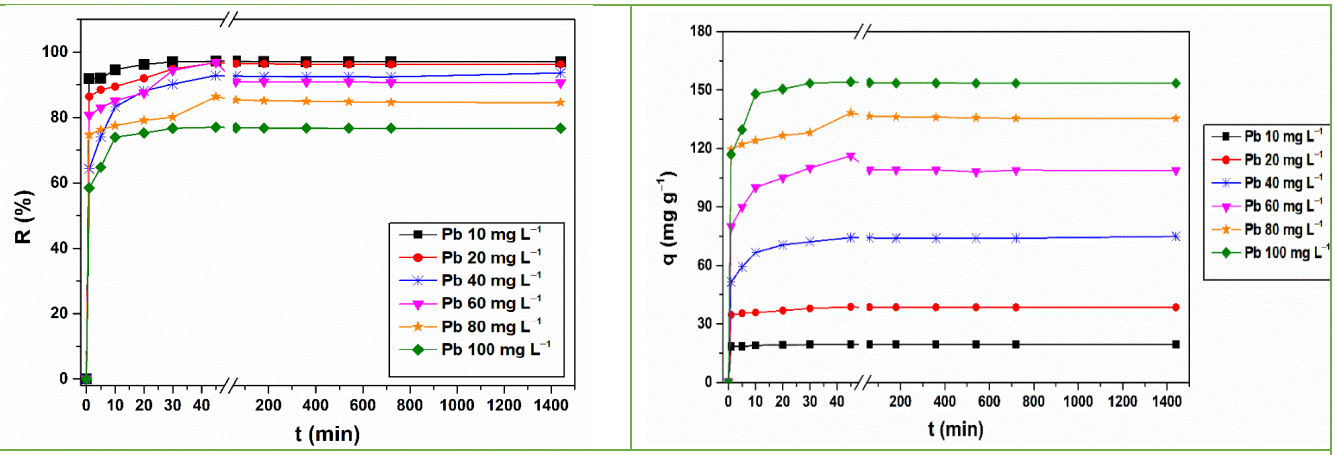

Pb

(a) **(c)**

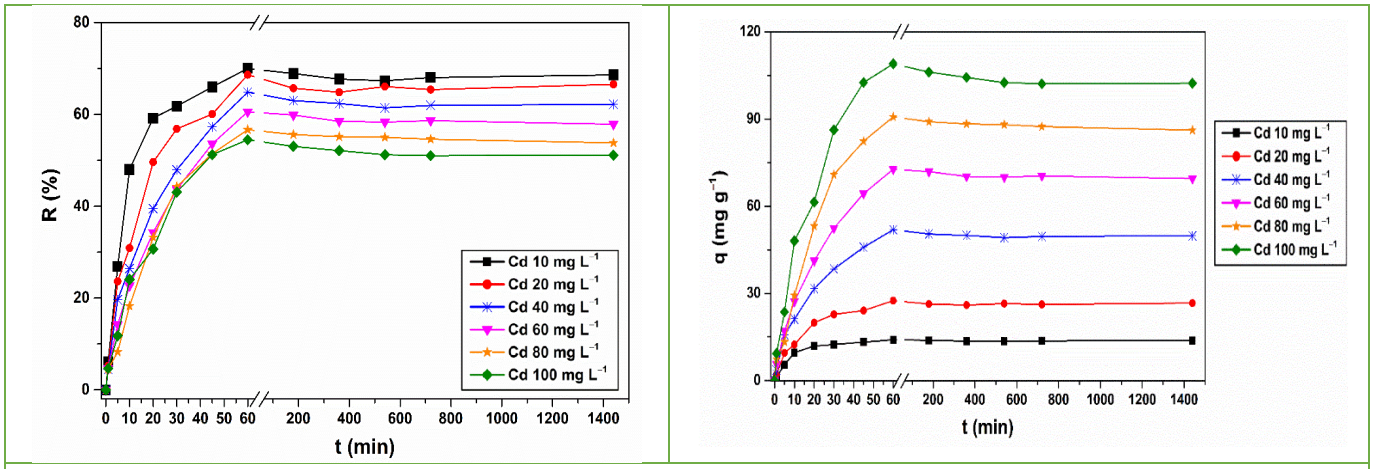

Figure 30. The effect of contact time on Pb and Cd removal efficiencies **(a,b)** and sorption capacities **(c,d)** of **CHIT-PAAA** (Ganea et al., 2022c).

Figure 31 displays the ANN architectures created for the adsorption models of both Pb and Cd onto **CHIT-PAAA**. The Levenberg–Marquardt algorithm was identified as the best appropriate method for modelling the adsorption processes of both metals. The algorithm selection was determined by identifying the highest R^2 values and the lowest MSEs ($R^2 = 0.999$ and MSE = 8.88 x 10^{-2} for Pb, $R^2 = 0.999$ and MSE = 7.89 x 10^{-2} for Cd). It was determined that the optimal number of concealed neurones was 5 for Pb sorption and 6 in the case of Cd sorption. The anticipated ANN outcomes closely aligned with the experimental data, indicating a strong fit and a low MSE.

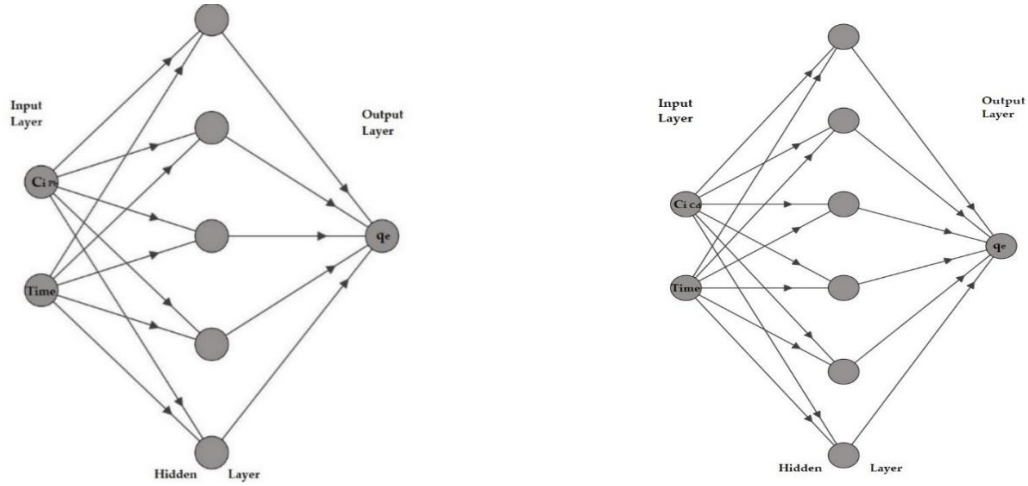

(a) **(b)**

Figure 31. ANN architectures for Pb **(a)** and Cd **(b)** adsorption modelling onto **CHIT-PAAA** (Ganea et al., 2022c)

3.2.1.6. Crosslinked Poly(benzofurane-co-arylacetic acid) ***PAAA-CL-XLD***

Preliminary sorption studies have been performed on the adsorption of tartrazine from stock solutions with **PAAA-*CL*-XLD**, however additional experiments are ongoing in order to establish the complete adsorption mechanism of this new material, especially by including the data also for **PAAA-*CL*-XLD_1**. The analysis on the data presented in **Figures 32 and 33** indicates that the adsorption efficiencies and capacities are higher for **PAAA-*CL*-XLD_2** than for **PAAA-*CL*-XLD_3**, most likely due to the inverse proportionality relationship between the particle size of the material and the specific surface area available to retain contaminants. In general, it can be noticed that at concentrations above 300 mg L^{-1}, the adsorption efficiency starts to decrease significantly. Also, it can be observed that no significant influence of contact time on dye adsorption is highlighted between 0.5–10 mg L^{-1}. However, for both materials, a gradual improvement in the tartrazine adsorption efficiency and sorption capacity is evidenced after increasing contact time at concentrations above 100 mg L^{-1}.

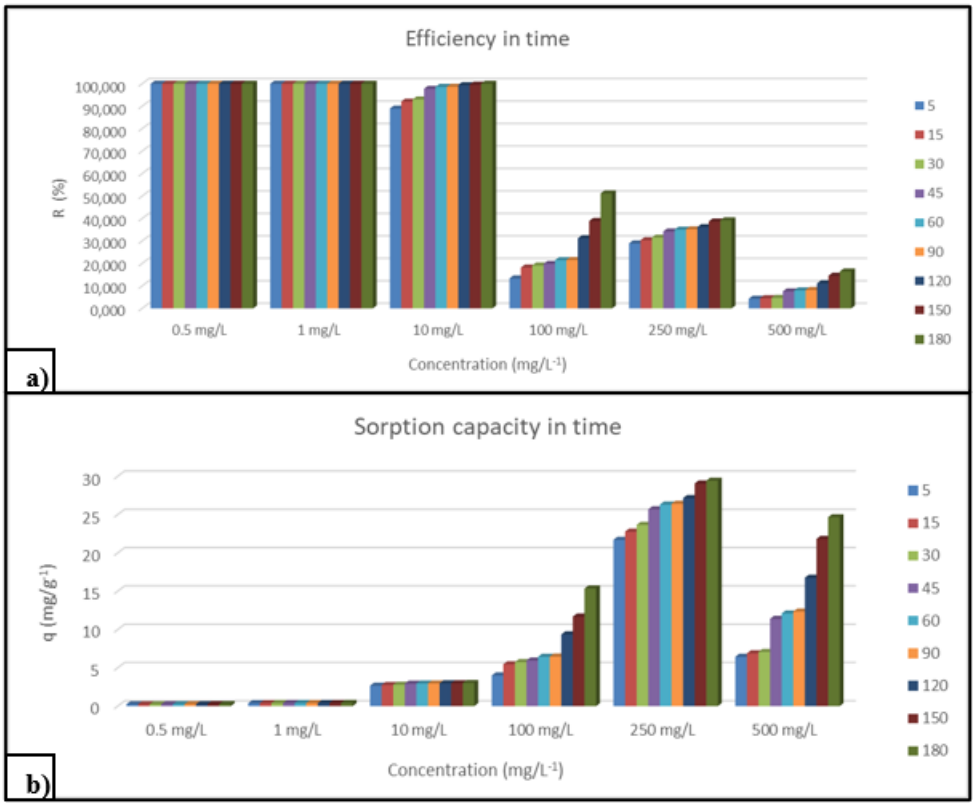

Figure 32. Effect of contact time on tartrazine removal efficiency **(a)** and sorption capacity **(b)** of **PAAA-*CL*-XLD_2**

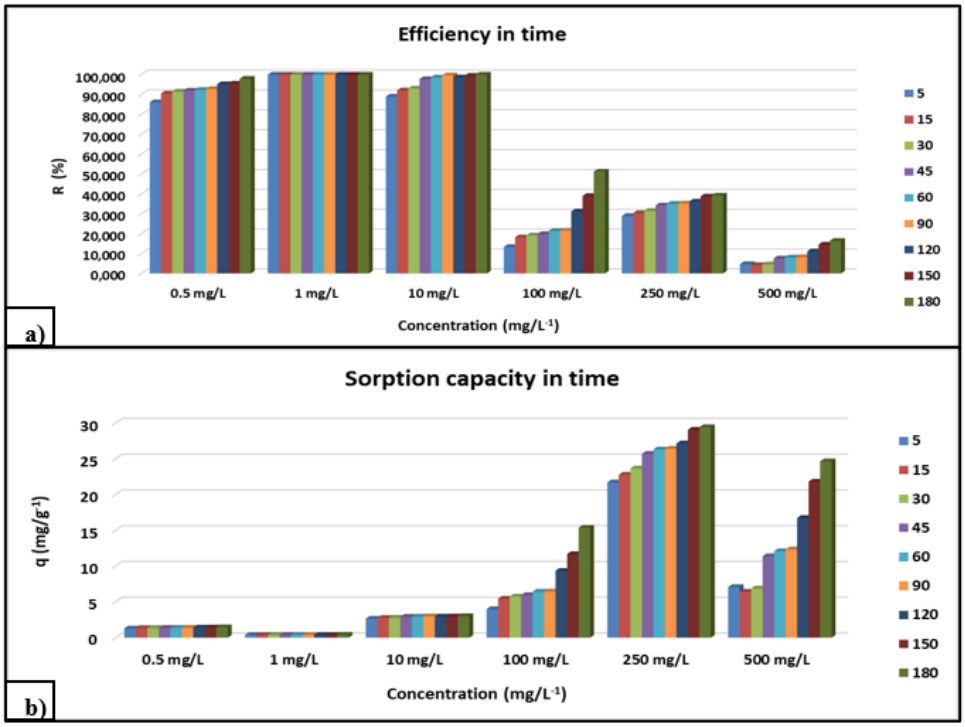

Figure 33. Effect of contact time on tartrazine removal efficiency **(a)** and sorption capacity **(b)** of **PAAA-*CL*-XLD_3**

*3.2.1.7. Modified Montmorillonite **MMT-PBAAA-DA***

The following findings regarding the adsorption experiments performed on **MMT-PBAAA-DA** were previously published in (Ganea et al., 2023a). **Figure 34** demonstrates that **MMT-PBAAA-DA** had remarkable efficacy in eliminating heavy metals from aqueous solutions. The new material exhibited high adsorption efficiencies for Cu, Pb, Cr, and Cd (90–100%) and intermediate efficiency for Mn, Ni, Zn, and Fe (69–87%). The best results were achieved for Pb (99.36% at 40 mg L^{-1} and 98.63% at 100 mg L^{-1}), whereas the minimal removal percentages were seen for Fe (69.94% at 40 mg L^{-1} and 64.83% at 100 mg L^{-1}). This fact is further emphasized by the values obtained for the sorption capacities. Consequently, the affinity of **MMT-PBAAA-DA** for heavy metals may be ranked as follows: Pb > Cr > Cd > Cu > Zn > Ni > Mn > Fe.

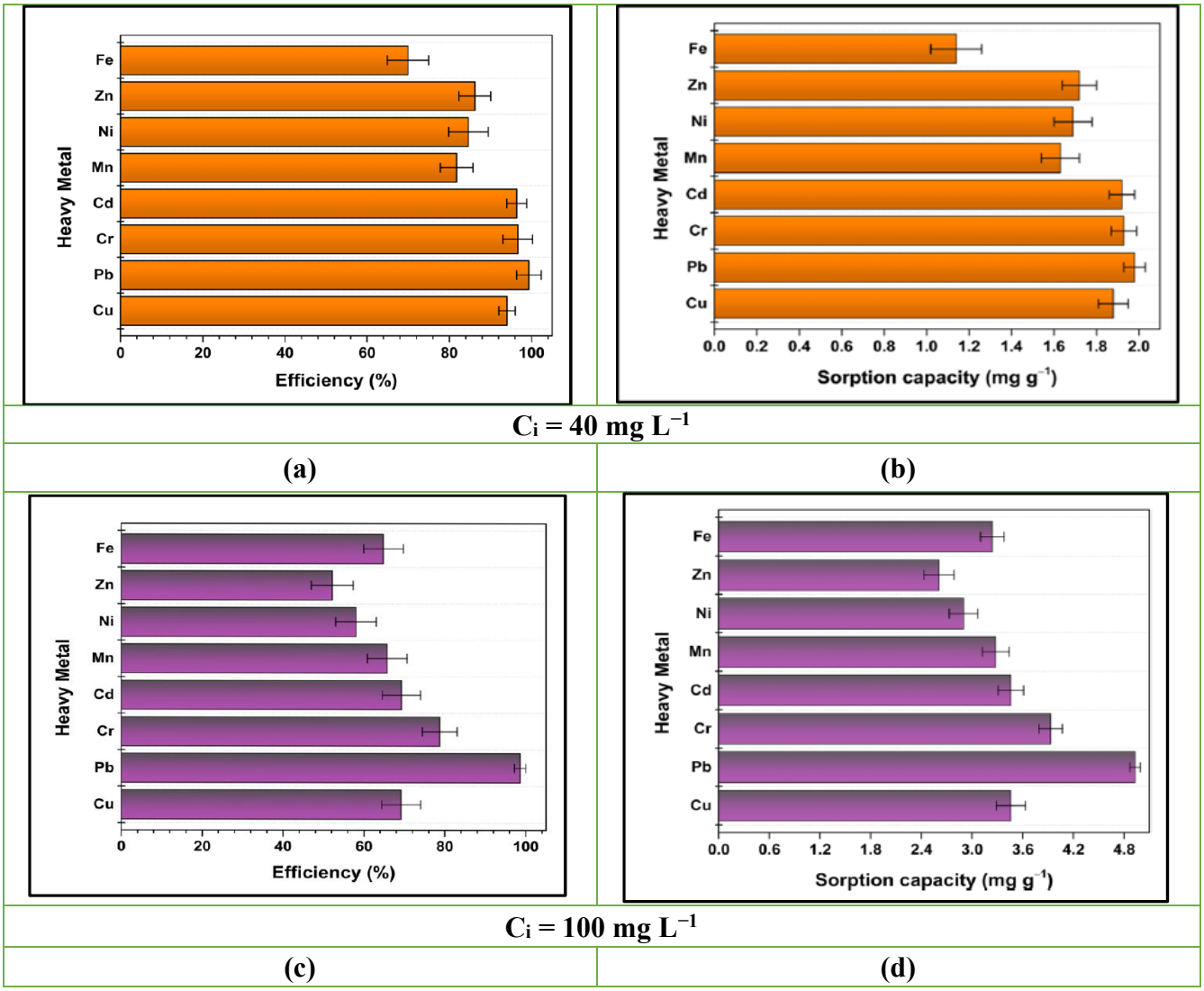

Figure 34. MMT-PBAAA-DA adsorption efficiency **(a,c)** and sorption capacity **(b,d)** at 40 mg L^{-1} and 100 mg L^{-1} concentration of heavy metals. (Ganea et al., 2023a)

Pb was selected for further equilibrium and kinetic experiments due to its superior adsorption efficiency on stock solutions. The Pb adsorption mechanism onto **MMT-PBAAA-DA** conformed well to both the Langmuir and Freundlich models. The adjusted correlation coefficient (Adj. R^2) and the difference between the estimated (q_e) and experimental (q_{e1}, q_{e2}) quantities of Pb adsorbed indicate that the pseudo-first-order kinetic model inadequately represents the adsorption process. Conversely, the pseudo-second-order kinetics more accurately aligns with the Pb sorption experimental data, emphasizing a direct connection between the site occupancy rate and the square of the number of free sites.

*3.2.1.8. Composite Based on Banana Peel and Stone Dust (**BPSD**)*

Preliminary tartrazine adsorption experiments were conducted on **BPSD** composite. However, additional tests are ongoing to completely characterize the sorption behaviour of this new material. Based on the preliminary adsorption tests carried out so far, it is observed that the adsorption efficiency and sorption capacity increase with the growth in the initial tartrazine concentration for both materials investigated (the simple stone dust **SD** and the new composite **BPSD)** (**Figures 35 and 36**). However, the organic food waste composite material **BPSD** recorded a better removal efficiency than stone dust, achieving to adsorb up to three times the amount of tartrazine compared to its primary constituent **SD**.

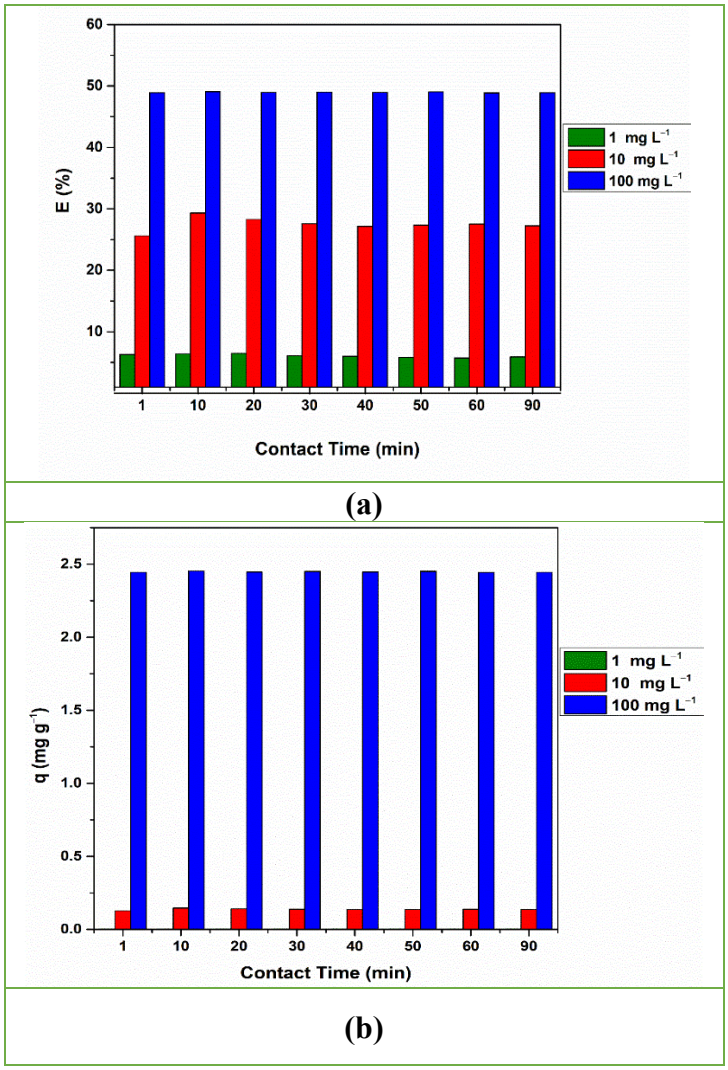

Figure 35. Effect of contact time on the tartrazine removal efficiency **(a)** and sorption capacity **(b)** of stone dust

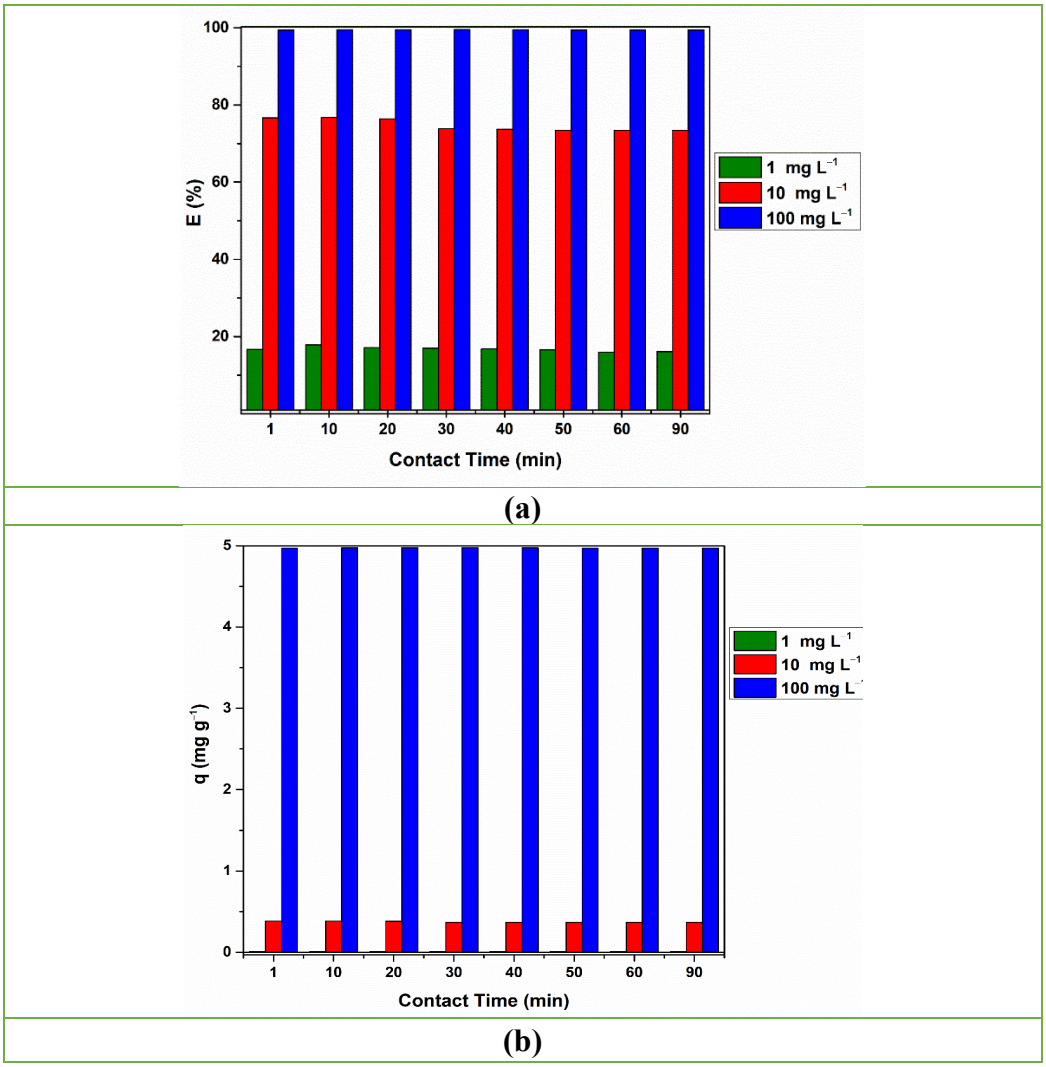

Figure 36. Effect of contact time on the tartrazine removal efficiency **(a)** and sorption capacity **(b)** of the newly synthesized composite **BPSD**

The lowest adsorption efficiencies were observed at a 1 mg L^{-1} concentration of tartrazine (16–18% for the banana peel-based composite and 5.7–6.5% for stone dust). At the initial concentration of 10 mg L^{-1} tartrazine, the **BPSD** composite had an adsorption efficiency three times higher than that of **SD** (73.4–76.7% for the food waste material compared to 25.6–29.3% for the dust). In contrast, at 100 mg L^{-1} tartrazine, the difference is almost double, with the composite registering an adsorption efficiency of 99.53% compared to stone dust, which retained only 49.06% of the dye present in solution. The influence of contact time on the tartrazine adsorption efficiency and sorption capacity of **BPSD** and **SD** revealed no significant variations, with the maximum peak efficiency attained after only 10–20 min, indicating a very fast retention rate of the examined dye.

*3.2.1.9. Composites Based on Watermelon Rind, Coffee Grounds (**WRCG**) and Stone Dust (**WRSD**)*

The watermelon-based composites **WRCG** and **WRSD** were the last ones to be synthesised, therefore only preliminary adsorption tests were performed so far. Additional ongoing laboratory experiments will soon provide a more comprehensive view on the crystal violet sorption mechanism of these waste-based composites. From the preliminary adsorption tests performed, it was observed that the sorption efficiency and capacity increase with the increment in the initial crystal violet concentration for both investigated composite materials (**Figures 37 and 38**). Overall, the composite material based on organic food residues **WRCG** has higher adsorption efficiencies than the one with the inorganic stone dust waste **WRSD**. Both composites recorded maximum sorption efficiencies (100% efficiency) at low concentrations of 0.5 mg L^{-1}, 1 mg L^{-1}, and 10 mg L^{-1} of crystal violet. The smallest values of the removal efficiencies were observed at 500 mg L^{-1} concentration of crystal violet (**WRCG** having between 33.3–91.04% efficacy and **WRSD** between 8.8–33%). The adsorption capacity of the composite materials ranged from 0.150-135.6 mg g^{-1} in the case of **WRCG** and from 0.150-50.2 mg g^{-1} for **WRSD**. It is noteworthy that after 90 minutes of contact, no significant changes in the adsorption efficiency of **WRCG** are observed. On the other hand, in the case of **WRSD** an upward trend is observed even after 180 minutes of contact. Thus, it can be stated that both composite materials can be successfully applied in crystal violet decontamination at low concentrations (< 10 mg L^{-1}), recording maximum adsorption efficiencies very quickly, after only 5 minutes of contact.

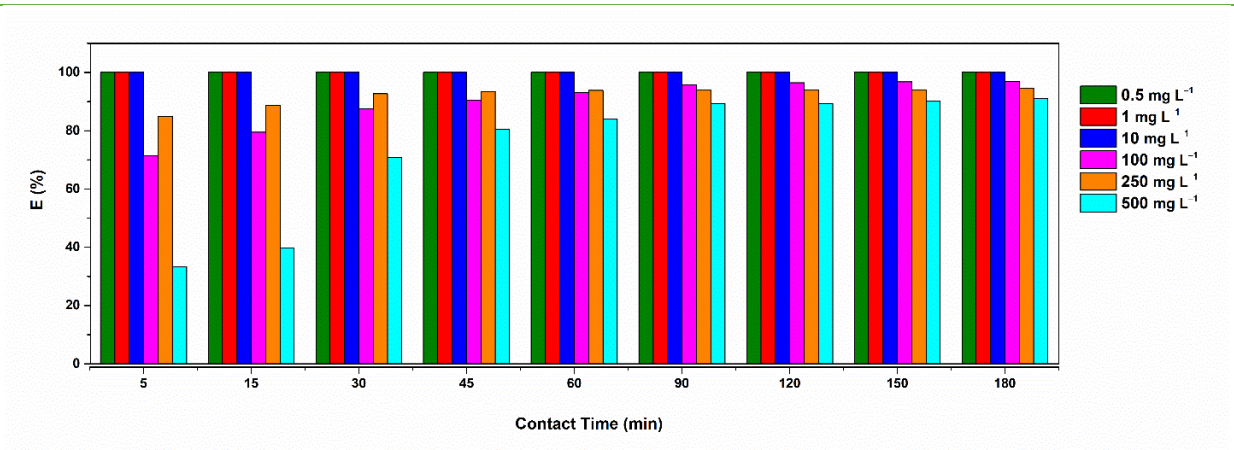

(a)

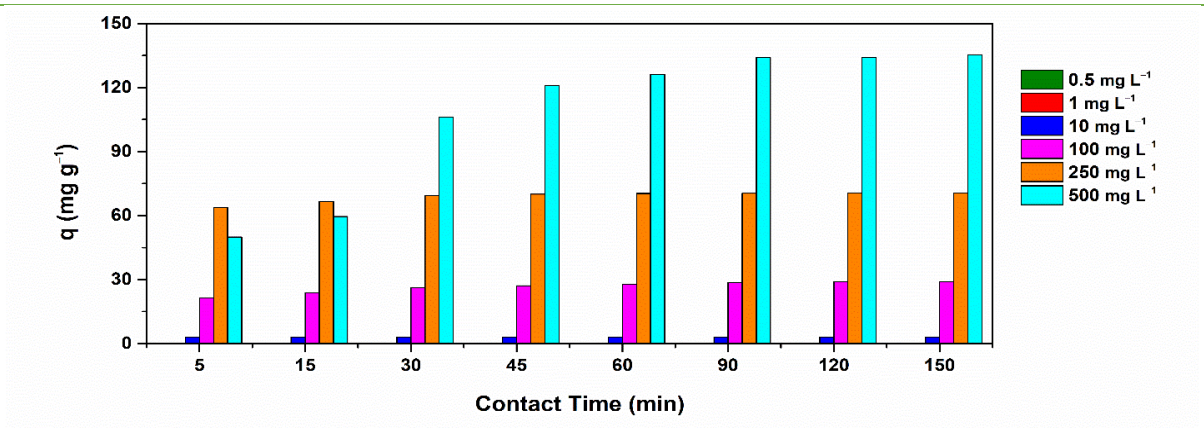

(b)

Figure 37. The effect of contact time on the crystal violet removal efficiency **(a)** and sorption capacity **(b)** of **WRCG** composite

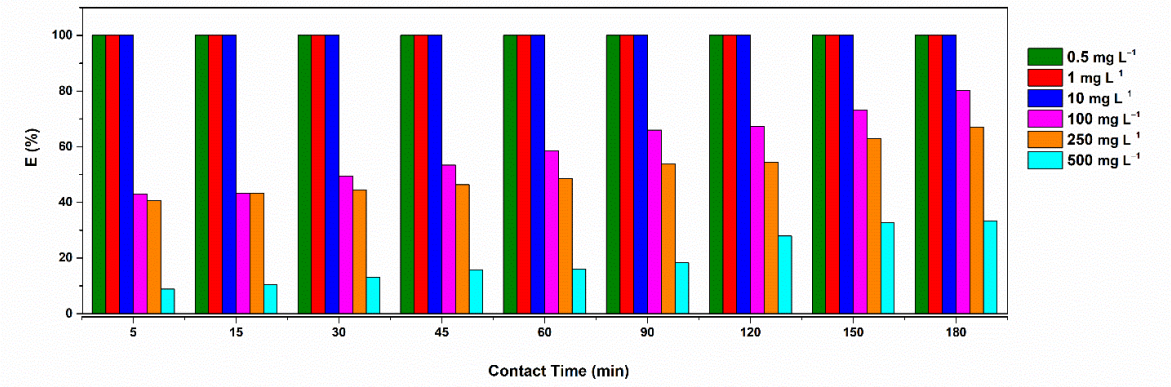

(a)

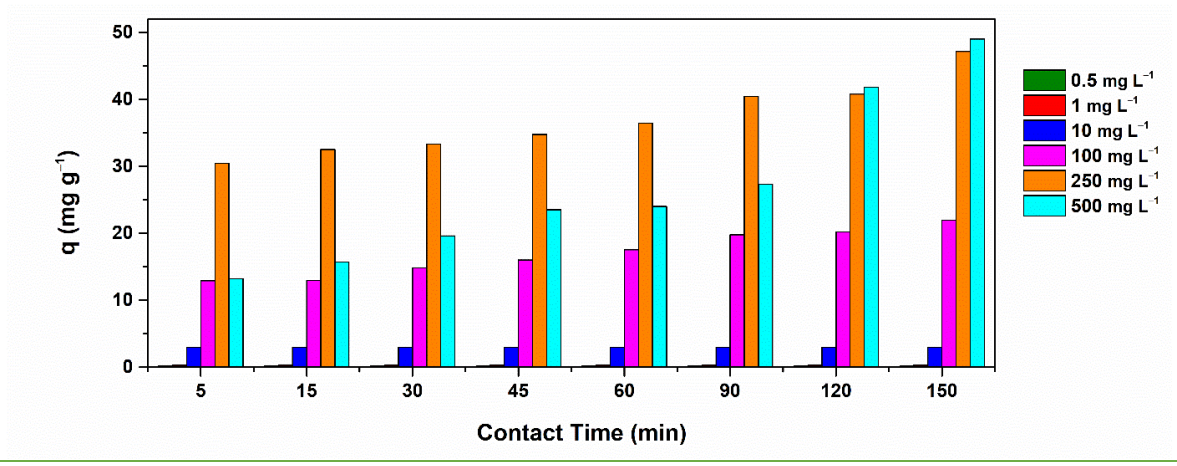

(b)

Figure 38. The effect of contact time on the crystal violet removal efficiency **(a)** and sorption capacity **(b)** of **WRSD** composite

3.2.2. Adsorption Experiments on Real-Life Water Samples Collected

*3.2.2.1. Magnetic Nanostructures **MNP@PAAA-NTA***

Figure 39 displays the results of the synthesized material **MNP@PAAA-NTA** efficiency in removing different heavy metals from P1 and P2 water samples collected from Roșia Montană area. It can be noticed that for P1 water sample (pH – 2.80), **MNP@PAAA-NTA** had good selectivity for Pb (60.99%), Cd (66.87%), Ni (29.29%), Fe (27.43%) and Cu (20.73%). On the other hand, all removal efficiencies were higher in the case of P2 water sample (pH – 2.52). Here, **MNP@PAAA-NTA** had high to very high efficiencies for Cr (100%), Cd (100%), Cu (98.36%), Fe (89.69%) and Sr (86.71%), but also for Mn (72.72%), Co (60.58%), Zn (51.84%), Al (31.35%) and Ni (26.68%). This demonstrates a better adsorption if the concentrations of metal ions that interfere in the sample are lower (Ganea et al., 2020).

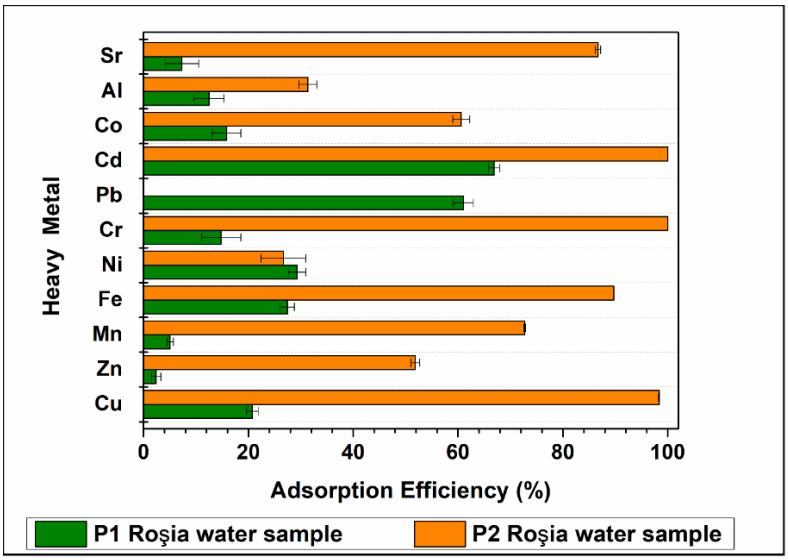

Figure 39. Adsorption efficiency of **MNP@PAAA-NTA** after performing tests on Roșia water samples were measured in 4 replicates (Ganea et al., 2020).

Comparing the content of heavy metals with the maximum permissible limits (MPL) of the Vth class of quality for surface waters (Romanian Ministerial Order 161/2006) – MPL-SW, it can be stated that both water samples exceed the allowed values in the case of Zn (8.300 mg L^{-1} for P1 and 2.431 mg L^{-1} for P2 compared to the MPL-SW of 1 mg L^{-1}), Cu (0.375 mg L^{-1} for P1 and 0.238 mg L^{-1} for P2 compared to MPL-SW), Mn (57.28 mg L^{-1} for P1 and 32.28 mg L^{-1} for P2 compared to MPL-SW of 1 mg L^{-1}), Fe (109.26 mg L^{-1} for P1 and 49.38 mg L^{-1} compared to MPL-SW of 2 mg L^{-1}), and Ni (0.25 mg L^{-1} for P1 and 0.12 mg L^{-1} for P2 compared to MPL-SW of 0.1 mg L^{-1}).

Moreover, exceeding of the MPLs is noted also for Cd and Co (0.03 mg L^{-1} and 0.17 mg L^{-1} compared to MPL-SW of 0.005 mg L^{-1} and 0.1 mg L^{-1}, respectively) in the case of P1 water sample. After performing the adsorption experiments, the metal contents were again compared with the MPLs. Although the concentrations decreased for all the investigated metal ions, the values still exceeded the regulatory exposure levels for surface waters in the case of Cu, Co, Zn, Mn, Fe, Ni, Cd (measured in P1 water sample) and of Zn, Mn and Fe (measured in P2 water sample). On the other hand, concentrations that complied with the regulatory exposure levels for metals in surface waters were obtained for Cu after applying **MNP@PAAA-NTA** on P2 water sample, reflecting the successful water treatment with our new material. Nevertheless, it is important to point out that significant changes occurred in the case of P2 water sample for Mn (decreasing from 32.28 mg L^{-1} to 8.806 mg L^{-1}) and Fe (decreasing from 49.38 mg L^{-1} to 5.087 mg L^{-1}), after applying the new magnetic nanomaterial (Ganea et al., 2020).

*3.2.2.2. Modified Chitosan **CHIT-PAAA***

Adsorption assays were performed on the collected-contaminated water samples after establishing the initial metal composition. Roșia Montană water samples registered significant amounts of Fe (11.48-460.81 mg L^{-1}), Mn (26.34-185.22 mg L^{-1}), Cu (0.06-1.55 mg L^{-1}) and Ni (0.24-0.89 mg L^{-1}), while Novăț-Borșa samples were rich in Fe (35.21-70.2 mg L^{-1}), Zn (1.77-50 mg L^{-1}), Cu (0.11- 0.94 mg L^{-1}) and Pb (0.01-0.40 mg L^{-1}). Each mining area had its specific metal composition profile as a result of the local geology and geochemistry, however, Roșia Montană water samples recorded higher metal concentrations as compared to Novăț-Borșa samples (Ganea et al., 2022c). On the other hand, excellent removal efficiencies (100%) were obtained for Ni, Pb, Cd and Cu in water samples collected from both locations (**Figure 40**). This fact indicates a better adsorption performance of **CHIT-PAAA** at low metal concentrations. Nonetheless, very good adsorption efficiencies were also determined for Fe (up to 95%) in Roșia Montană water samples and Zn (up to 85%) in Novăț-Borșa samples (Ganea et al., 2022c).

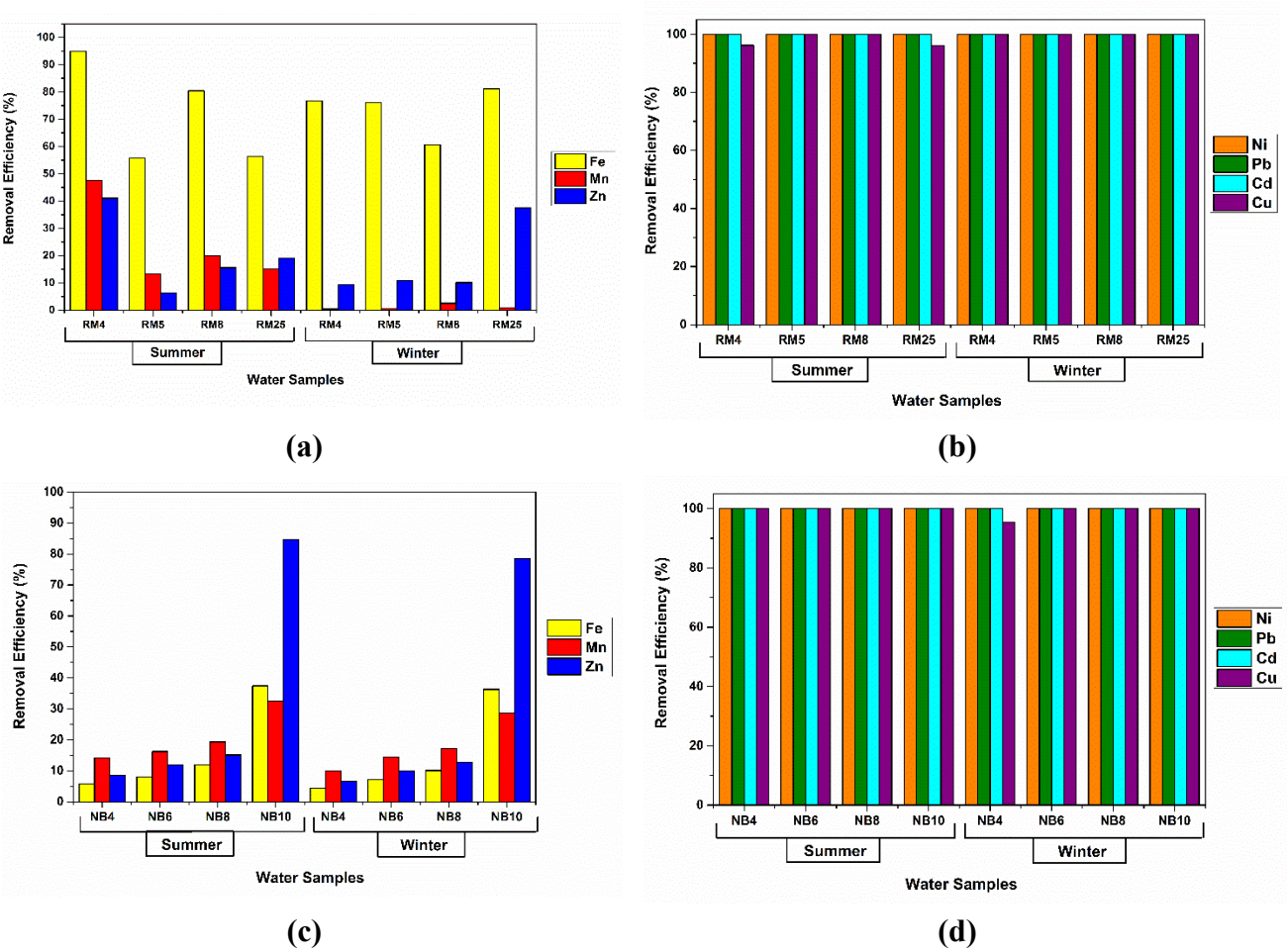

Figure 40. CHIT-PAAA removal efficiencies for heavy metals in water samples from Roșia Montană **(a,b)** and Novăț-Borșa **(c,d)** Mining Areas, Romania (Ganea et al., 2022c).

*3.2.2.3. Modified Montmorillonite **MMT-PBAAA-DA***

Figure 41 displays the heavy metals concentrations determined in the metal-contaminated water samples and the results on the removal efficiency of the synthesized material on these samples. After comparing the heavy metal concentrations measured in the two samples with the regulatory exposure levels (Cu 0.1 mg L^{-1}, Zn 1 mg L^{-1}, Mn 1 mg L^{-1}, Fe 2 mg L^{-1}, Ni 0.1 mg L^{-1}, Pb 0.25 mg L^{-1}, Cr 0.05 mg L^{-1} and Cd 0.005 mg L^{-1}) for the fifth class of quality in surface waters (Romanian Ministerial Order 161/2006), exceeding of the limits was noticed in the case of Cu (0.586 mg L^{-1} for AMD1 and 0.15 mg L^{-1} for AMD2), Zn (4.133 mg L^{-1} for AMD1 and 0.262 mg L^{-1} for AMD2), Mn (51.9 mg L^{-1} for AMD1 and 5.301 mg L^{-1} for AMD2), Fe (48.61 mg L^{-1}

for AMD1 and 4.119 mg L^{-1} for AMD2) and Cd (0.062 mg L^{-1} for AMD1 and 0.035 mg L^{-1} for AMD2). Moreover, Ni determined in AMD1 sample (0.535 mg L^{-1}) also exceeded the allowed limits (Ganea et al., 2023a).

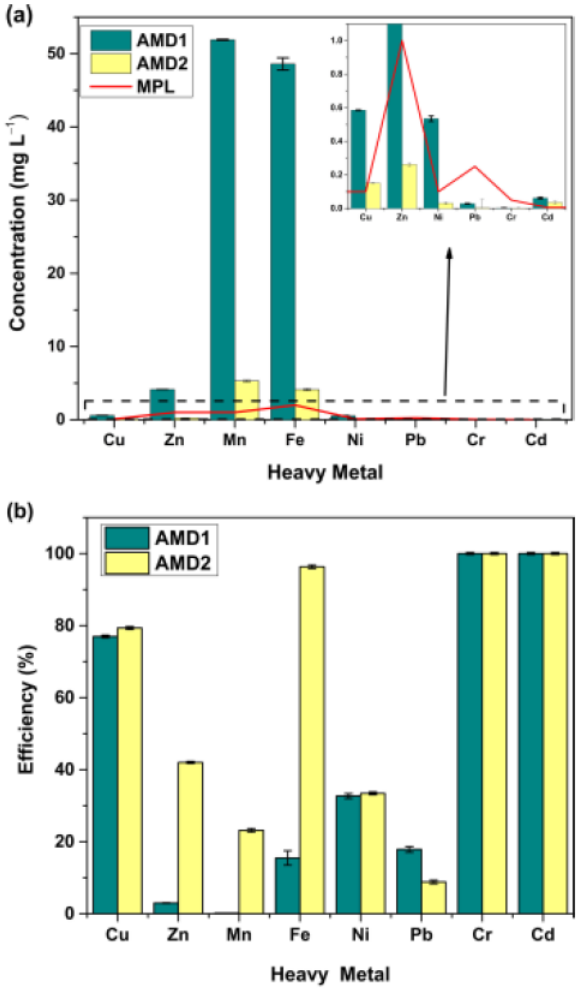

Figure 41. (a) Heavy metal concentrations in the water samples from Roșia Montană and **(b) MMT-PBAAA-DA** adsorption efficiency on the real contaminated samples. (Ganea et al., 2023a)

MMT-PBAAA-DA exhibited high adsorption for Cr (100%), Cd (100%), Cu (77–79%) and Fe (96 %) (**Figure152b**). The material performances were generally better for AMD2 than AMD1, most probably due to the lower metal concentrations registered. After performing the adsorption experiments, the concentrations for Cd in AMD1 and Cu, Zn and Cd in AMD2 decreased below the maximum permissible limits, highlighting the good impact this material can have on water quality (Ganea et al., 2023a).

4. CONCLUSIONS

The present thesis focused on the development, synthesis, and performance evaluation of novel materials designed for the adsorption of contaminants, particularly heavy metals and organic dyes, from aqueous solutions. The primary objective of this work was to explore four distinct categories of materials, each synthesized through "green chemistry" methods, to investigate their chemical, structural and morphological properties and to assess their effectiveness in removing pollutants from contaminated aqueous solutions with the aim of providing sustainable alternatives to traditional water treatment solutions. The materials included in this research are: eco-innovative nanostructures (magnetic nanostructures **MNP@PAAA-NTA, MNP@PAAA-DA, MNP@PAAA-FA** and polymeric nanostructures **ZD** and **ZT)**, sustainable biopolymers (modified chitosan **CHIT-PAAA** and crosslinked poly(benzofurane-co-arylacetic acid **PAAA-*CL*-XLD**), environmentally-friendly mineral composites (modified montmorillonite **MMT-PBAAA-DA**) and circular waste-based composites (based on banana peel and stone dust (**BPSD**), watermelon rind and coffee grounds (**WRCG**) and watermelon rind and stone dust (**WRSD**)). The synthesized hybrid materials were characterized by various techniques, including TEM-SEM-EDX, TGA, DLS, VSM, XRPD, XPS, ss-NMR, BET, DLS and Zeta Potential Analysis, which confirmed their chemical, structural and morphological properties, providing essential information about their potential effectiveness as adsorbents. The diversity of functional groups and the simple separation through filtration, centrifugation or external magnetic fields recommends these new cost-effective, and sustainable materials for applications in wastewater decontamination. The various functional groups (hydroxyl, carboxyl, amine, lactones, phenols, etc.) identified through the characterization methods applied, provide many opportunities to link or immobilize contaminants.

These hybrid materials were assessed in regard to their potential to adsorb heavy metals and synthetic organic dyes from aqueous solutions. The effect of different parameters such as initial contaminant concentration, pH and contact time on the adsorption efficiency of the materials were analysed to characterize the sorption behaviour of the materials. Experimental adsorption records were investigated employing different isotherm models (Langmuir, Freundlich, Temkin, Dubinin-Radushkevich, Khan, Redlich-Peterson, Sips, Khan, Toth and Koble-Corrigan) in both linear and nonlinear regression and four kinetic models (Pseudo-first order, Pseudo-second order kinetics, Weber-Morris Intra-particle Diffusion and Elovich). Furthermore, 3D adsorption rate models and

artificial neural networks (ANNs) were also generated to characterize the adsorption process. In the end, several materials were also tested for heavy metals adsorption from metal-contaminated surface waters collected from two former mining areas in Romania.

The batch adsorption experiments on the magnetic nanostructures **MNP@PAAA-NTA** showed showed good efficiency in removing Cr (100%), Cd (100%), Cu (98.36%), Fe (89.7%), Sr (86.71%), Mn (72.72%), Co (60.58%), Zn (51.84%) from real-life contaminated water samples, thus exhibiting good performances in metal ions water decontamination which is making it suitable for applications in water and wastewater treatment. It was also demonstrated that the heavy metals removal efficiency and sorption capacity decreased at higher metal concentrations (Ganea et al., 2020. **MNP@PAAA-DA** exhibited different behaviour based on the metal adsorbed and the initial concentration of the pollutant: Cu (14.75−62.26%), Mn (1.74−28.09%) and Zn (1.77−20.89%). It was noticed that adsorption occurs in the first 30 min, after which no important modifications intervene. The pH experiments showed an increasing trend in the adsorption capacity in alkaline environments, as a result of the negative surface charge appearing due to the deprotonation of hydroxyl groups on the magnetite. In the case of **MNP@PAAA-FA**, maximum crystal violet removal efficiency (92.75%) was obtained after only 30 min, indicating that adsorption occurs very fast on this material, equilibrium being reached after 180 min of contact. The adsorption capacity is linearly proportional to the initial crystal violet concentration, reaching a maximum of 25.12 mg g^{-1} at 125 mg L^{-1}, Therefore, we can conclude that the complex structure of these magnetic nanostructures can interconnect and retain the dye molecules through several types of interactions, such as electrostatic, π–π stacking interaction, etc., playing an essential role in the adsorption mechanism. The reusability of **MNP@PAAA-FA** was also investigated, exceptional dye removal efficiency (88.74%) being still observed upon completion of 10 cycles of adsorption-desorption (Ganea et al., 2021). The preliminary metal sorption studies conducted on the zein-based nanostructures **ZD** and **ZT** demonstrated that there were no significant differences in the efficiency obtained after 5 min and 4 h of contact time. The Fe sorption tests suggest that these polymeric nanostructures exhibit inferior removal efficiencies at low concentrations compared to their primary constituent, **zein**. **ZT** recorded retention efficiencies of more than 60% at concentrations of 75 and 100 mg^{-1} Fe, while **ZD** had 40% efficiency. The chitosan-based composite material (**CHIT-PAAA**) exhibited excellent performance in the removal of heavy metals. Successful results were achieved regarding in retaining Pb (96.07%-100%), Cd (76.71%-100%), Fe (95%), Zn (85%),

Ni (100%), Cu (100%) from both batch solutions and contaminated mining water samples. Maximum adsorption was reached fast, after only 45 minutes of contact time for Pb and 60 minutes for Cd. The 3D, equilibrium and kinetic models suggest that the sorption capacity of **CHIT-PAAA** is directly dependent on the contact time and initial metal concentrations, and chemisorption is the rate-limiting process. Similar results were generated with the neural network architectures developed, highlighting a high level of trust in the ANN models for both Pb and Cd adsorption. The recyclability of the copolymer in 7 adsorption-desorption cycles showed that the removal efficiency decreased from 97.18% to 89% for Pb and from 70% to 58% for Cd (Ganea et al., 2022c). The preliminary tartrazine sorption tests on the crosslinked polymer **PAAA-*CL*-XLD** indicated that the adsorption efficiencies and capacities are higher for **PAAA-*CL*-XLD_2** than for **PAAA-*CL*-XLD_3**, most likely due to the inverse proportionality relationship between the particle size of the material and the specific surface area available to retain contaminants. No significant influence of contact time on the dye adsorption efficiency and sorption capacity of this material was noticed between 0.5–10 mg L^{-1} initial concentration of tartrazine. The modified montmorillonite **MMT-PBAAA-DA** exhibited remarkable efficacy in eliminating heavy metals from aqueous solutions. The new material exhibited high adsorption efficiencies for Cu, Pb, Cr, and Cd (90–100%) and medium efficiency for Mn, Ni, Zn, and Fe (69–87%). The best results were achieved for Pb (99.36% at 40 mg L^{-1} and 98.63% at 100 mg L^{-1}), while minimal removal percentages were seen for Fe (69.94% at 40 mg L^{-1} and 64.83% at 100 mg L^{-1}). This hybrid material presented good removal performances also on the metal-contaminated surface water samples collected from Roșia Montană area (up to 100%), with selectivity especially for Cr, Cd, Cu, Zn and Fe. The changes in the physicochemical parameters were also significant, highlighting the high increase in the pH values of the investigated water samples, fitting them between the maximum permissible limits established in the Romanian legislation for surface waters. The composite based on banana peel and stone dust **BPSD** recorded a better removal efficiency (99.53%) than stone dust (29.3%), achieving a dye retention three times higher compared to the amount of tartrazine adsorbed by its primary constituent **SD.** The influence of contact time on the tartrazine adsorption efficiency and sorption capacity of **BPSD** and **SD** revealed no significant variations, with the maximum peak efficiency attained after only 10–20 min, indicating a very fast retention rate of the examined dye. In general, the watermelon-based composite **WRCG** recorded higher crystal violet adsorption efficiencies than the inorganic stone dust waste **WRSD**. However,

at low crystal violet concentrations (0.5 mg L^{-1}-10 mg L^{-1}) both composites registered maximum sorption efficiencies (100%) very quickly, after only 5 min of contact.

The findings from the equilibrium studies show that each material has a different behaviour. The adsorption mechanism of **MNP@PAAA-DA** is described by the Freundlich model, whereas for **MNP@PAAA-FA,** Khan isotherm most accurately represents the adsorption. In the case of **CHIT-PAAA**, Sips and Koble-Corrigan isotherms fit the best, while for **MMT-PBAAA-DA** the experimental data exhibited a better fit to the Langmuir isotherm (Ganea et al., 2023a). The kinetics investigation showed that in general, the pseudo-second-order model was found more appropriate for the characterization of the contaminants adsorption processes onto all synthesized materials, defining chemisorption as the rate-limiting step and indicating a proportionality between the occupation rate of the adsorption sites and the square number of available sites.

While these results are promising, several areas remain to be optimized and expanded for further research. Future studies could focus on enhancing the adsorption capacity and selectivity of these materials by modifying their surface chemistry or incorporating additional functional groups to target specific contaminants. Moreover, the scalability of the synthesis methods should be investigated to ensure that these materials can be produced at a large scale for industrial applications. Finally, exploring the reintegration of the used adsorbents into other economic sectors could offer a circular economy solution by reusing the materials after they have adsorbed contaminants. One potential application is in the construction field, where adsorbents can be repurposed as building materials into the production of walls or bitumen for road construction. Additionally, another interesting avenue for future research lies in agriculture, where adsorbents that have accumulated essential metals (such as zinc, copper, or manganese) during the adsorption process could be used as fertilizers, being critical for plant growth. These applications could greatly enhance the environmental sustainability and economic feasibility of the hybrid materials, making them not only effective adsorbents but also valuable resources for other industries.

Overall, the current thesis presents significant contributions to the field of water remediation, specifically in the development of novel sustainable hybrid materials designed for the adsorption of contaminants such as heavy metals and organic dyes from aqueous solutions. This work contributes to the development of sustainable solutions through green chemistry methods for the protection of water resources, supporting efforts to achieve global sustainability goals and ensuring cleaner water for future generations.

BIBLIOGRAPHY

1. Ahuja, S., 2021, Handbook of Water Purity and Quality. In S. Ahuja (Ed.), Handbook of Water Purity and Quality (2nd Edition). Elsevier. https://doi.org/10.1016/C2019-0-01203-4
2. Balaram, V., Copia, L., Kumar, U. S., Miller, J., & Chidambaram, S., 2023, Pollution of water resources and application of ICP-MS techniques for monitoring and management—A comprehensive review. Geosystems and Geoenvironment, 2(4), 100210. https://doi.org/10.1016/J.GEOGEO.2023.100210
3. Barnhart, J., 1997, Occurrences, Uses, and Properties of Chromium. Regulatory Toxicology and Pharmacology, 26(1), S3–S7. https://doi.org/10.1006/RTPH.1997.1132
4. Bennett, B. G., 1982, Exposure of man to environmental nickel — An exposure commitment assessment. Science of The Total Environment, 22(3), 203–212. https://doi.org/10.1016/0048-9697(82)90065-1
5. Bilal, M., Ihsanullah, I., Younas, M., & Ul Hassan Shah, M., 2021, Recent advances in applications of low-cost adsorbents for the removal of heavy metals from water: A critical review. Separation and Purification Technology, 278, 119510. https://doi.org/10.1016/J.SEPPUR.2021.119510
6. Booth, C. A., & Charlesworth, S. M., 2014, Water resources in the built environment: Management issues and solutions. In Water Resources in the Built Environment: Management Issues and Solutions (Vol. 9780470670910). Wiley Blackwell. https://doi.org/10.1002/9781118809167
7. Carpenter, S. R., Caraco, N. F., Corell, D. L., Howarth, R. W., Sharpley, A. N., & Smith, V. H., 1998, Nonpoint pollution of surface waters with phosphorus and nitrogen. Ecological Applications - Ecological Society of America, 9(3), 559–568. https://doi.org/10.1038/SCIENTIFICAMERICAN0894-62
8. Chandra, V., Park, J., Chun, Y., Lee, J. W., Hwang, I. C., & Kim, K. S., 2010, Water-dispersible magnetite-reduced graphene oxide composites for arsenic removal. ACS Nano, 4(7), 3979–3986. https://doi.org/10.1021/NN1008897/SUPPL_FILE/NN1008897_SI_002.AVI
9. Crini, G., & Lichtfouse, E., 2018, Green Adsorbents for Pollutant Removal (G. Crini & E. Lichtfouse, Eds.; Vol. 19). Springer Cham. https://doi.org/10.1007/978-3-319-92162-4
10. Crini, G., 2006, Non-conventional low-cost adsorbents for dye removal: A review. Bioresource Technology, 97(9), 1061–1085. https://doi.org/10.1016/J.BIORTECH.2005.05.001
11. Crini, G., Lichtfouse, E., Wilson, L. D., & Morin-Crini, N., 2019, Conventional and non-conventional adsorbents for wastewater treatment. Environmental Chemistry Letters, 17(1), 195–213. https://doi.org/10.1007/S10311-018-0786-8/FIGURES/5
12. Ding, L., Zou, B., Gao, W., Liu, Q., Wang, Z., Guo, Y., Wang, X., & Liu, Y., 2014, Adsorption of Rhodamine-B from aqueous solution using treated rice husk-based activated carbon.

Colloids and Surfaces A: Physicochemical and Engineering Aspects, 446, 1–7. https://doi.org/10.1016/J.COLSURFA.2014.01.030
13. Dotto, G. L., Esquerdo, V. M., Vieira, M. L. G., & Pinto, L. A. A., 2012, Optimization and kinetic analysis of food dyes biosorption by Spirulina platensis. Colloids and Surfaces B: Biointerfaces, 91(1), 234–241. https://doi.org/10.1016/J.COLSURFB.2011.11.008
14. Du Plessis, A., 2023, Water Resources from a Global Perspective. 1–25. https://doi.org/10.1007/978-3-031-24019-5_1
15. Dutta, S., Adhikary, S., Bhattacharya, S., Roy, D., Chatterjee, S., Chakraborty, A., Banerjee, D., Ganguly, A., Nanda, S., & Rajak, P., 2024, Contamination of textile dyes in aquatic environment: Adverse impacts on aquatic ecosystem and human health, and its management using bioremediation. Journal of Environmental Management, 353, 120103. https://doi.org/10.1016/J.JENVMAN.2024.120103
16. El Mahdaoui, A., Radi, S., Elidrissi, A., Faustino, M. A. F., Neves, M. G. P. M. S., & Moura, N. M. M., 2024, Progress in the modification of cellulose-based adsorbents for the removal of toxic heavy metal ions. Journal of Environmental Chemical Engineering, 12(5), 113870. https://doi.org/10.1016/J.JECE.2024.113870
17. Esrey, S. A., Potash, J. B., Roberts, L., & Shiff, C., 1991, Effects of improved water supply and sanitation on ascariasis, diarrhoea, dracunculiasis, hookworm infection, schistosomiasis, and trachoma. Bulletin of the World Health Organization, 69(5), 609–621.
18. European Commission, 2000, Water Framework Directive 2000/60/EC. European Commission. https://eur-lex.europa.eu/eli/dir/2000/60/oj/eng
19. Freundlich, H., 1907, Über die absorption in lösungen. Zeitschrift Für Physikalische Chemie- Stöchiometrie Und Verwandschaftslehre, 57, 385–470.
20. Ganea, I. V., Nan, A., Roba, C., & Baciu, C., 2023a, Characterization of a Neoteric Clay-Based Composite for the Removal of Heavy Metals from Mining Water. Analytical Letters, 56(2), 257–271. https://doi.org/10.1080/00032719.2022.2051713
21. Ganea, I. V., Nan, A., Roba, C., Neamțiu, I., Gurzău, E., Turcu, R., Filip, X., & Baciu, C., 2022c, Development of a New Eco-Friendly Copolymer Based on Chitosan for Enhanced Removal of Pb and Cd from Water. Polymers, 14(18). https://doi.org/10.3390/polym14183735
22. Ganea, I.-V., & Nan, A., 2023b, Composite material based on organic food waste and its preparation procedure for environmental protection applications. OSIM.
23. Ganea, I.-V., & Nan, A., 2024, Sustainable composite based on recycled food waste and its preparation procedure. OSIM.
24. Ganea, I.-V., 2018, Reducing exposure to heavy metals from contaminated water by applying new synthesized materials based on poly(benzofurane-co-arylacetic acid) [Master's Thesis]. Babes-Bolyai University.
25. Ganea, I.-V., Nan, A., & Turcu, R., 2022a, Copolymer based on chitosan and synthesis procedure (Patent No. 133503/29.04.2022.). OSIM. https://ro.espacenet.com/publicationDetails/originalDocument?FT=D&date=20220429&DB=&locale=ro_RO&CC=RO&NR=133503B1&KC=B1&ND=4

26. Ganea, I.-V., Nan, A., & Turcu, R., 2022b, Magnetic nanostructures based on polymer functionalized with chelated agents (Patent No. 134031/30.09.2022). OSIM. https://ro.espacenet.com/publicationDetails/originalDocument?FT=D&date=20220930&DB=&locale=ro_RO&CC=RO&NR=134031B1&KC=B1&ND=5
27. Ganea, I.-V., Nan, A., & Turcu, R., 2023c, Montmorillonite modified with poly(benzofurane-co-arylacetic) acid functionalized with dopamine (Patent Patent No. 133609/30.01.2023). OSIM. https://ro.espacenet.com/publicationDetails/originalDocument?FT=D&date=20230130&DB=&locale=ro_RO&CC=RO&NR=133609B1&KC=B1&ND=4
28. Ganea, I.-V., Nan, A., Baciu, C., & Turcu, R., 2021, Effective removal of crystal violet dye using neoteric magnetic nanostructures based on functionalized poly(benzofuran-co-arylacetic acid): Investigation of the adsorption behaviour and reusability. Nanomaterials, 11(3), 1–15. https://doi.org/10.3390/nano11030679
29. Ganea, I.-V., Nan, A., Turcu, R., Roba, C., Neamtiu, I. A., & Baciu, C., 2020, Study of Metal Ion Removal from Aqueous Systems Using Magnetic Nanostructures Based on Functionalized Poly(Benzofuran-co-Arylacetic Acid). Analytical Letters, 54(1–2), 184–203. https://doi.org/10.1080/00032719.2020.1737100
30. Geerten, J. I. S., 1998, Drinking Water Supply and Agricultural Pollution (G. J. I. Schrama, Ed.; 1st Edition). Springer Dordrecht. https://doi.org/10.1007/978-94-011-5106-1
31. Georgopoulos, P. G., Roy, A., Yonone-Lioy, M. J., Opiekun, R. E., & Lioy, P. J., 2001, ENVIRONMENTAL COPPER: ITS DYNAMICS AND HUMAN EXPOSURE ISSUES. Journal of Toxicology and Environmental Health Part B: Critical Reviews, 4(4), 341–394. https://doi.org/10.1080/109374001753146207
32. Godt, J., Scheidig, F., Grosse-Siestrup, C., Esche, V., Brandenburg, P., Reich, A., & Groneberg, D. A., 2006, The toxicity of cadmium and resulting hazards for human health. Journal of Occupational Medicine and Toxicology, 1(1), 1–6. https://doi.org/10.1186/1745-6673-1-22/TABLES/1
33. Government of Romania, 2023, Ordinance No. 7 from 18/01/2023 on the quality of water intended for human consumption. Government of Romania. https://legislatie. just.ro/Public/ DetaliiDocument/264337
34. Guechi, E. K., & Hamdaoui, O., 2016, Evaluation of potato peel as a novel adsorbent for the removal of Cu (II) from aqueous solutions: equilibrium, kinetic, and thermodynamic studies. Desalination and Water Treatment, 57(23), 10677–10688. https://doi.org/ 10.1080/19443994.2015.1038739
35. Haddaway, N. R., Page, M. J., Pritchard, C. C., & McGuinness, L. A., 2022, PRISMA2020: An R package and Shiny app for producing PRISMA 2020-compliant flow diagrams, with interactivity for optimised digital transparency and Open Synthesis. Campbell Systematic Reviews, 18(2), e1230. https://doi.org/https://doi.org/10.1002/cl2.1230
36. Hall, R. P., Van Koppen, B., & Van Houweling, E., 2014, The Human Right to Water: The Importance of Domestic and Productive Water Rights. Science and Engineering Ethics, 20(4), 849–868. https://doi.org/10.1007/S11948-013-9499-3/TABLES/1

37. Haque, E., Lo, V., Minett, A. I., Harris, A. T., & Church, T. L., 2013, Dichotomous adsorption behaviour of dyes on an amino-functionalised metal–organic framework, amino-MIL-101(Al). Journal of Materials Chemistry A, 2(1), 193–203. https://doi.org/10.1039/C3TA13589F
38. Ho, Y. S., & McKay, G., 2000, The kinetics of sorption of divalent metal ions onto sphagnum moss peat. Water Research, 34, 735–742. https://doi.org/http://doi.org/10.1016/S0043-1354(99)00232-8
39. Hussain, M. K., Khatoon, S., Nizami, G., Fatma, U. K., Ali, M., Singh, B., Quraishi, A., Assiri, M. A., Ahamad, S., & Saquib, M., 2024, Unleashing the power of bio-adsorbents: Efficient heavy metal removal for sustainable water purification. Journal of Water Process Engineering, 64, 105705. https://doi.org/10.1016/J.JWPE.2024.105705
40. Hussain, M., Riaz, A., Zeb, H., Ali, A., Mujahid, R., Ahmad, F., & Zafar, M. S., 2025, Paving the path to water security: The role of advanced adsorbents in wastewater treatment. Journal of Water Process Engineering, 71, 107333. https://doi.org/10.1016/J.JWPE.2025.107333
41. Hutzinger, O., Barcelo, D., & Kostianoy, A., 2009, The Handbook of Environmental Chemistry Volume 5 - Water Pollution (O. Hutzinger, D. Barcelo, & A. Kostianoy, Eds.; Vol. 5). Springer - Verlag
42. Jain, A. K., Gupta, V. K., Bhatnagar, A., & Suhas., 2003, Utilization of industrial waste products as adsorbents for the removal of dyes. Journal of Hazardous Materials, 101(1), 31–42. https://doi.org/10.1016/S0304-3894(03)00146-8
43. Janaki, V., Oh, B. T., Shanthi, K., Lee, K. J., Ramasamy, A. K., & Kamala-Kannan, S., 2012, Polyaniline/chitosan composite: An eco-friendly polymer for enhanced removal of dyes from aqueous solution. Synthetic Metals, 162(11–12), 974–980. https://doi.org/10.1016/J.SYNTHMET.2012.04.015
44. Jiang, H., Wu, S., & Zhou, J., 2023, Preparation and modification of nanocellulose and its application to heavy metal adsorption: A review. International Journal of Biological Macromolecules, 236, 123916. https://doi.org/10.1016/J.IJBIOMAC.2023.123916
45. Johnson, L. B., 1968, Letter to the President of the Senate and to the Speaker of the House Transmitting an Assessment of the Nation's Water Resources. The American Presidency Project. https://www.presidency.ucsb.edu/documents/letter-the-president-the-senate-and-the-speaker-the-house-transmitting-assessment-the
46. Kacsó, T., Neaga, I. O., Erincz, A., Astete, C. E., Sabliov, C. M., Oprean, R., & Bodoki, E., 2018, Perspectives in the design of zein-based polymeric delivery systems with programmed wear down for sustainable agricultural applications. Polymer Degradation and Stability, 155, 130–135. https://doi.org/10.1016/j.polymdegradstab.2018.07.014
47. Kumar, A., Kumar, V., & Singh, J., 2019, Role of Fungi in the Removal of Heavy Metals and Dyes from Wastewater by Biosorption Processes. 397–418. https://doi.org/10.1007/978-3-030-25506-0_16
48. Lagergren, S., & Sven, K., 1898, Zur theorie der sogennanten adsorptiongeloster stoffe. Kungliga Sevenska Vetenskapsakademiens. Handlingar, 24, 1–39.
49. Langmuir, I., 1918, The constitution and fundamental properties of solids and liquids. J. Am. Chem. Soc., 40, 1361–1403.

50. Lehr, J. H., Keeley, J. W., & Lehr, J., 2005, Water Encyclopedia: Domestic, municipal, and industrial water supply and waste disposal (J. H. Lehr, J. W. Keeley, & J. Lehr, Eds.). Wiley Interscience. https://www.wiley.com/en-au/Water+Encyclopedia% 2C+Volume+1%2C+ Domestic%2C+Municipal%2C+and+Industrial+Water+Supply+and+Waste+Disposal-p-978047 1736875
51. Lerner, K. L., & Lerner Wilmoth, B., 2005a, U•X•L Encyclopedia of water science (K. Lee. Lerner & B. Wilmoth. Lerner, Eds.; Vol. 3). Thomson Gale.
52. Lichtfouse, E., Schwarzbauer, J., & Robert, D., 2012, Environmental chemistry for a sustainable world vol. 2: Remediation of Air and Water Pollution. In E. Lichtfouse, J. Schwarzbauer, & D. Robert (Eds.), Environmental Chemistry for a Sustainable World (Vol. 2). Springer Dordrecht. https://doi.org/10.1007/978-94-007-2439-6/COVER
53. Liu, L., Gao, Z. Y., Su, X. P., Chen, X., Jiang, L., & Yao, J. M., 2015, Adsorption removal of dyes from single and binary solutions using a cellulose-based bioadsorbent. ACS Sustainable Chemistry and Engineering, 3(3), 432–442. https://doi.org/10.1021/ SC500848M/SUPPL_FILE/SC500848M_SI_001.PDF
54. Liu, Y., Wu, S. H., Hua, C., & Han, X., 2014, Effect of synergistic sorption of Cr(VI) and Mn(II) in aqueous solution using magnetic nanoparticles. Desalination and Water Treatment, 52(22–24), 4183–4189. https://doi.org/10.1080/19443994.2013.801794
55. Malik, P. K., 2004, Dye removal from wastewater using activated carbon developed from sawdust: adsorption equilibrium and kinetics. Journal of Hazardous Materials, 113(1–3), 81–88. https://doi.org/10.1016/J.JHAZMAT.2004.05.022
56. Malmqvist, B., & Rundle, S., 2002, Threats to the running water ecosystems of the world. Environmental Conservation, 29(2), 134–153. https://doi.org/10.1017/S0376892902000097
57. Mekala, D., Davidson, B., Samad, M., & Boland, A.-M., 2008, Wastewater Reuse and Recycling Systems: A Perspective into India and Australia (128; IWMI Working Paper).
58. Molden, D., 2007, Water for food, Water for Life: A Comprehensive Assessment of Water Management in Agriculture. https://archive.iwmi.org/assessment/ files_new/synthesis/ Summary_SynthesisBook.pdf
59. Musie, W., & Gonfa, G., 2023, Fresh water resource, scarcity, water salinity challenges and possible remedies: A review. In Heliyon (Vol. 9, Issue 8). Elsevier Ltd. https://doi.org/10.1016/j.heliyon.2023.e18685
60. Nan, A., Bunge, A., Cîrcu, M., Petran, A., Hădade, N. D., & Filip, X., 2017, Poly(benzofuran-co-arylacetic acid)-a new type of highly functionalized polymers. Polymer Chemistry, 8(22), 3504–3514. https://doi.org/10.1039/c7py00523g
61. Nan, A., Filip, X., & Liebscher, J., 2024, Reaction of Lactone-Containing Poly(benzofuran-co-arylacetic acid) with Diamines to Cross-Linked Products of Improved Thermal Conductivity. Molecules, 29(24), 6020. https://doi.org/10.3390/MOLECULES29246020/S1
62. Negulescu, M., Antoniu, R., Rusu, G., & Cuşa, E., 1982, Protecția Calității Apelor (M. Negulescu, R. Antoniu, G. Rusu, & E. Cuşa, Eds.). Tehnică, Ed.

63. Nejadshafiee, V., & Islami, M. R., 2019, Adsorption capacity of heavy metal ions using sultone-modified magnetic activated carbon as a bio-adsorbent. Materials Science and Engineering: C, 101, 42–52. https://doi.org/10.1016/J.MSEC.2019.03.081
64. Norton, M., Lane, A., & Ryan, S., 2018, Water Resources: A New Water Architecture. Wiley-Blackwell.
65. Parliament of Romania, 1996, Waters Law No. 107 from 25/09/1996. Parliament of Romania. https://legislatie.just.ro/Public/DetaliiDocument/8565
66. Parliament of Romania, 2002, Law No. 458 from 08/07/2002 on drinking water. Parliament of Romania. https://legislatie.just.ro/Public/DetaliiDocument/37723
67. Parliament of Romania, 2004, Law No. 311 from 28/06/2004 amending and supplementing Law no. 458/2002 on drinking water quality. Parliament of Romania. https://legislatie.just.ro/Public/DetaliiDocument/53106
68. Pham, V. H. T., Kim, J., Chang, S., & Chung, W., 2022, Bacterial Biosorbents, an Efficient Heavy Metals Green Clean-Up Strategy: Prospects, Challenges, and Opportunities. Microorganisms 2022, Vol. 10, Page 610, 10(3), 610. https://doi.org/10.3390/MICROORGANISMS10030610
69. Rees, M., 2010, The Reith Lectures - Scientific Horizons. BBC Radio 4 - The Reith Lectures. https://www.bbc.co.uk/programmes/b00sk5nc/episodes/player
70. Rijsberman, F. R., 2006, Water scarcity: Fact or fiction? Agricultural Water Management, 80(1–3), 5–22. https://doi.org/10.1016/J.AGWAT.2005.07.001
71. Saleh, T. A., 2024, Materials, nanomaterials, nanocomposites, and methods used for the treatment and removal of hazardous pollutants from wastewater: Treatment technologies for water recycling and sustainability. Nano-Structures & Nano-Objects, 39, 101231. https://doi.org/10.1016/J.NANOSO.2024.101231
72. Santos, S. C. R., & Boaventura, R. A. R., 2008, Adsorption modelling of textile dyes by sepiolite. Applied Clay Science, 42(1–2), 137–145. https://doi.org/10.1016/J.CLAY.2008.01.002
73. Temkin, M. J., & Pyzhev, V., 1940, Kinetics of ammonia synthesis on promoted iron catalysts. Acta Physicochim. URSS, 12, 217–222.
74. The World Economic Forum, 2025, The Global Risks Report 2025 20th Edition. www.weforum.org
75. Török, B., & Dransfield, T., 2017, Green Chemistry: An Inclusive Approach. In B. Török & T. Dransfield (Eds.), Green Chemistry (1st Edition). Elsevier. http://www.sciencedirect.com:5070/book/9780128092705/green-chemistry
76. United Nations Environment Programme, 2019, Global Environment Outlook 6. https://www.unep.org/resources/global-environment-outlook-6
77. United Nations Water, 2021, Summary Progress Update 2021: SDG 6 - Water and sanitation for all. https://www.unwater.org/sites/default/files/app/uploads/2021/12/SDG-6-Summary-Progress-Update-2021_Version-July-2021a.pdf
78. United Nations, 2015, Sustainable Development Goal (SDG) 6: Clean Water and Sanitation. Sustainable Development Goals. https://sdgs.un.org/goals/goal6

79. United Nations' General Assembly, 2010, The human right to water and sanitation: resolution A/RES/64/292. UN,. https://digitallibrary.un.org/record/687002
80. United States Environmental Protection Agency (US EPA), 1972, The Clean Water Act (CWA). In The Federal Water Pollution Control Act 33 U.S.C. §1251 (pp. 1–233). United State Environmental Protection Agency (US EPA). https://www.govinfo.gov/content/pkg/USCODE-2018-title33/pdf/USCODE-2018-title33-chap26.pdf
81. United States Environmental Protection Agency (US EPA), 1974, Safe Drinking Water Act (SDWA). In Safe Drinking Water Act 42 U.S.C. § 300f. United States Environmental Protection Agency (US EPA). https://www.epa.gov/sdwa
82. Velusamy, S., Roy, A., Sundaram, S., & Kumar Mallick, T., 2021, A Review on Heavy Metal Ions and Containing Dyes Removal Through Graphene Oxide-Based Adsorption Strategies for Textile Wastewater Treatment. The Chemical Record, 21(7), 1570–1610. https://doi.org/10.1002/TCR.202000153
83. Vijayaraghavan, K., & Balasubramanian, R., 2015, Is biosorption suitable for decontamination of metal-bearing wastewaters? A critical review on the state-of-the-art of biosorption processes and future directions. Journal of Environmental Management, 160, 283–296. https://doi.org/10.1016/J.JENVMAN.2015.06.030
84. WaterAid, & Tearfund., 2001, The Human Waste: A Call for Urgent Action to Combat the Millions of Deaths Caused by Poor Sanitation. https://washmatters.wateraid.org/publications/the-human-waste-report-a-call-for-urgent-action-to-combat-the-millions-of-deaths
85. World Health Organization (WHO), 2017, World health statistics 2017: monitoring health for the SDGs, sustainable development goals. https://www.who.int/publications/i/item/9789241565486
86. Wrobel, L. C., & Brebbia, C. A., 1991, Water Pollution: Modelling, Measuring and Prediction (L. C. Wrobel & C. A. Brebbia, Eds.). Springer Dordrecht. https://doi.org/10.1007/978-94-011-3694-5
87. Xu, X., Gao, B. Y., Yue, Q. Y., & Zhong, Q. Q., 2010, Preparation and utilization of wheat straw bearing amine groups for the sorption of acid and reactive dyes from aqueous solutions. Journal of Hazardous Materials, 182(1–3), 1–9. https://doi.org/10.1016/J.JHAZMAT.2010.03.071
88. Yang, S. T., Chen, S., Chang, Y., Cao, A., Liu, Y., & Wang, H., 2011, Removal of methylene blue from aqueous solution by graphene oxide. Journal of Colloid and Interface Science, 359(1), 24–29. https://doi.org/10.1016/J.JCIS.2011.02.064
89. Zhang, Z., Chen, Y., Wang, D., Yu, D., & Wu, C., 2023, Lignin-based adsorbents for heavy metals. Industrial Crops and Products, 193, 116119. https://doi.org/10.1016/J.INDCROP.2022.116119
90. Zhao, G., Li, J., Ren, X., Chen, C., & Wang, X., 2011, Few-layered graphene oxide nanosheets as superior sorbents for heavy metal ion pollution management. Environmental Science and Technology, 45(24), 10454–10462. https://doi.org/10.1021/ES203439V/SUPPL_FILE/ES203439V_SI_001.PDF